Constitutive behavior of asymmetric multi-material honeycombs with bi-level variably-thickened composite architecture

M. Awasthi[a], S. Naskar[b], A. Singh[a], T. Mukhopadhyay[b,*]

[a] *Department of Aerospace Engineering, Indian Institute of Technology Kanpur, Kanpur, India*
[b] *Faculty of Engineering and Physical Sciences, University of Southampton, Southampton, UK*

Abstract

Bi-level tailoring of cellular metamaterials involving a dual design space of unit cell and elementary beam level architectures has recently gained traction for the ability to achieve extreme elastic constitutive properties along with modulating multi-functional mechanical behavior in an unprecedented way. This article proposes an efficient analytical approach for the accurate evaluation of all constitutive elastic constants of asymmetric multi-material variably-thickened hexagonal lattices by considering the combined effect of bending, stretching, and shearing deformations of cell walls along with their rigid rotation. A tri-member unit cell is conceptualized, wherein all nine constitutive constants are obtained through the mechanics under one cell wall direction and subsequent repetitive coordinate transformations. We enhance the design space of lattice metamaterials substantially here by introducing multiple exploitable dimensions such as asymmetric geometry, multi-material unit cells and variably-thickened cell walls, wherein the conventional monomaterial auxetic and non-auxetic hexagonal configurations can be analyzed as special cases along with other symmetric and asymmetric lattices such as a range of rectangular and rhombic geometries. The generic analytical approach along with extensive numerical results presented in this paper opens up new avenues for efficient optimized design of the next-generation multi-functional lattices and cellular metamaterials with highly tailored effective elastic properties.

Keywords: Asymmetric honeycombs; Multi-material lattices; Programmable elastic moduli; Cellular metamaterials; Auxetic and non-auxetic lattices; Lattice derivatives

1. Introduction

Metamaterials deal with global mechanical properties with periodic micro-structural design and intrinsic material distribution at the micro-scale, wherein the interplay between geometry and mechanics can bring about wonders in terms of effective physical properties [1]. Over the last decade, this field of architected materials has received tremendous attention from the research community for the prospect of achieving unprecedented mechanical properties beyond the limits of conventional materials along with tunable multi-functional abilities such as extreme effective elastic moduli and stiffness [2, 3, 4, 5, 6, 7], negative Poisson's ratio [8, 9, 10, 11, 12], programmable constitutive behavior [13, 14, 15, 16], high specific energy absorption capability [17, 18, 19, 20, 21], active modulation of mechanical

*Corresponding author: T. Mukhopadhyay (Email address: t.mukhopadhyay@soton.ac.uk)

properties [1, 22, 23, 24], shape morphing [25, 26, 27, 28, 29, 30], unusual acoustic parameters (for example, negative refractive index) [31], energy harvesting [32, 33], vibration control [34, 35, 36] etc. In practical design scenarios, most of these metamaterials need to possess multifunctionalities such as specific energy absorption, specific strength and stiffness, stability and dynamic characteristics. Many of these properties are also interrelated; for example, the dynamic and stability characteristics are dependent on different stiffness components, while the specific energy absorption can be evaluated based on the force-displacement or stress-strain constitutive behavior. For these reasons, we have briefly discussed some of the other relevant features of mechanical metamaterials as a part of the literature review. Subsequently, we focus more on the aspect of elastic moduli and the constitutive behavior of mechanical metamaterials. Concerning the design of metamaterials in general, due to intense investigation of different unit cell level geometries over the last few years, the aspect of solely periodic unit cell design for lattices have started to saturate. There exists a strong rationale to introduce new dimensions in lattice metamaterial designs, which is the central focus of this paper.

Artificially engineered materials with the ability of possessing passive and active programmability in mechanical behavior to an extreme extent, along with the recent advancement in additive manufacturing, have provided us with tremendous opportunities to enhance the performance of multiple technologically demanding engineering sectors like aerospace, mechanical, civil and biomedical industries [1]. In the following discussion, we provide a very brief review of relevant research activities in the field of lattice metamaterials that primarily deal with effective elastic properties. Analytical expressions for the effective elastic moduli of regular hexagonal lattices (refer to Figure 1(a)) were derived based on a unit cell approach considering periodic boundary conditions [37]. In such honeycomb structures, unusual effective negative Poisson's ratio (i.e. auxetic behavior), or zero Poisson's ratio can be obtained by intuitively modifying the hexagonal unit cell architecture [38]. Unit cell based periodic lattices have been proposed to have extreme specific stiffness based on anti-curvature lattices [39, 40] and topology-optimized cell walls [5], non-invariant elastic properties [41] and on-demand elastic property modulation [22, 42, 43, 44]. Effective elastic properties of monomaterial asymmetric honeycombs were investigated in [45, 46]. Formulations presented in the current work are influenced by these papers, wherein multiple new exploitable dimensions would be introduced. Thickened joints in convenstional hexagonal unit cell were shown to provide more strength based on optimized geometries [47]. The utilization of buckling-induced instability has led to an enhanced energy absorption capacity and strain rate dependent constitutive behavior [48]. Wei et al. [49] have proposed a lightweight cellular metastructure incorporating coupled tailorable thermal expansion and tunable Poisson's ratio. A theoretical and nu-

merical investigation has been proposed by Wang et al. [50] for a hybrid hierarchical square honeycomb to investigate effective in-plane elastic properties and their tailorable features. Ling et al. [51] have presented an additively manufactured mechanical metamaterial with large magnitude of Poisson's ratio. Further, apart from static properties, a range of unprecedented mechanical properties can be obtained in metamaterials under dynamics conditions, for example, negative Young's modulus [6], negative shear modulus [52], negative mass density [53], elastic cloaks [54] and negative bulk modulus [55]. It may be noted here that analyzing lattice-like structural forms is relevant and useful to multiple length scales (nano to macro) covering naturally-occurring and artificial materials and structures [56, 57, 58, 59].

From the existing literature, it becomes evident that physical properties of intrinsic materials and metamaterials are defined at two different length scales. Intrinsic materials properties of constituent elements at the micro-scale generally depend upon chemical composition, atomic and molecular structures of the material. Another set of material properties related to equivalent macro-scale behavior can be defined in metamaterials where the macroscale effective properties become a function of the intrinsic material properties and the microstructural lattice geometry. The key factor for a metamaterial remains that the relative length scales of the microstructural dimension of the periodic units and the overall lattice dimensions should have a significant difference. However, the interplay of mechanical properties of the intrinsic materials, geometry and the concerning mechanics can offer unparalleled opportunities for novel material design. Generally, a unit cell-based approach is adopted to design lattice metamaterials with a single type of intrinsic material [37] (refer to Figure 1(a, d)). Recently, multi-material lattices have been proposed where different cell walls in the unit cells have different intrinsic material properties (refer to Figure 1(b)) [60]. With the progress of multi-material additive manufacturing, such lattices can be physically realized with adequate precision [61, 62, 63, 64, 65]. In the present study, to expand the design space further, we would introduce asymmetry in the unit cell architecture of multi-material lattices as shown in Figure 1(c). In such periodic bending-dominated architectures, we notice that the unit cell level periodic boundary conditions can be satisfied by considering the cell wall (i.e. the connecting beams) to have rotationally restrained supports at the two ends (refer to [41, 66]). In such a scenario, the bending moment along the beam length reduces as we move away from the two ends of a beam, and becomes zero at the mid-point. To exploit such insights in optimizing material utilization, we would further introduce beam-level variably- thickened architectures along with unit cell geometries (which we refer to as bi-level design), indicated in Figure 3(a). Thus, the salient features of the current work can be summarized as the compound effect of multi-material unit cells, asymmetric unit cell geometry, and beam-level variably-thickened architecture. This work aims to derive an effi-

cient and insightful analytical approach for obtaining the effective elastic properties involving the entire constitutive matrices of such architected composite lattices.

To the best knowledge of the authors, no study has been presented to date that deals with the analytical formulations concerning entire constitutive matrices for asymmetric multi-material variably-thickened honeycomb structures. Based on the discussions presented in the preceding paragraphs, it becomes evident that the development of an analytical solution for accurately and efficiently determining the mechanical properties including bending, stretching, and shearing deformations of cell walls along with their rigid rotation would be crucial for achieving multifunctional properties and further muli-objective design optimizations. In this article, we will primarily focus on hexagonal asymmetric geometries, the special cases of which can be readily deduced as conventional non-auxetic and auxetic hexagonal lattices, rhombic and rectangular lattices with different architectures (refer to Figure 1(g)).

We would follow a bottom-up approach for analyzing the effective elastic properties of lattice metamaterials here. The local deformation behavior of the elementary beams is accounted for in the analysis considering bending, shear and axial deformations. Note that we propose to introduce beam-level architectures at this stage, as shown later in Fig. 3(b). Subsequently, a unit cell, comprised of multi-material variably-thickened beam elements, is analyzed for deriving the closed-form expressions of the effective in-plane elastic moduli. We introduce the effect of asymmetry at the unit cell level. At a higher length scale, such lattices are adopted for structural applications depending on their effective elastic constitutive behavior (refer to Figure 1(a-f)).

The overarching contribution of this paper lies in enhancing the conventional design space of lattice metamaterials substantially by introducing multiple exploitable dimensions such as (1) asymmetric geometry, (2) composite multi-material unit cells, (3) variably-thickened cell walls (derived through physics-based rationale) and (4) their coupled effect, wherein the traditional monomaterial auxetic and non-auxetic configurations (symmetric and asymmetric) can be analyzed as special cases. Hereafter the paper is organized as follows. In section 2, the generalized analytical formulation is presented for determining the equivalent material properties of multi-material variably-thickened asymmetric lattices. We have derived all elements of the elastic constitutive matrices, unlike most reported studies in this field. Subsequently, we show how to obtain the elastic moduli in different directions from the elastic constitutive matrices. The section 3 is dedicated to extensive validation considering a range of material distribution and unit cell architectures, followed by a detailed numerical investigation concerning the geometrical parameters of the bi-level architecture and multi-material properties. Finally, the most interesting findings of the present study are summarized in the section 4 along with concluding remarks.

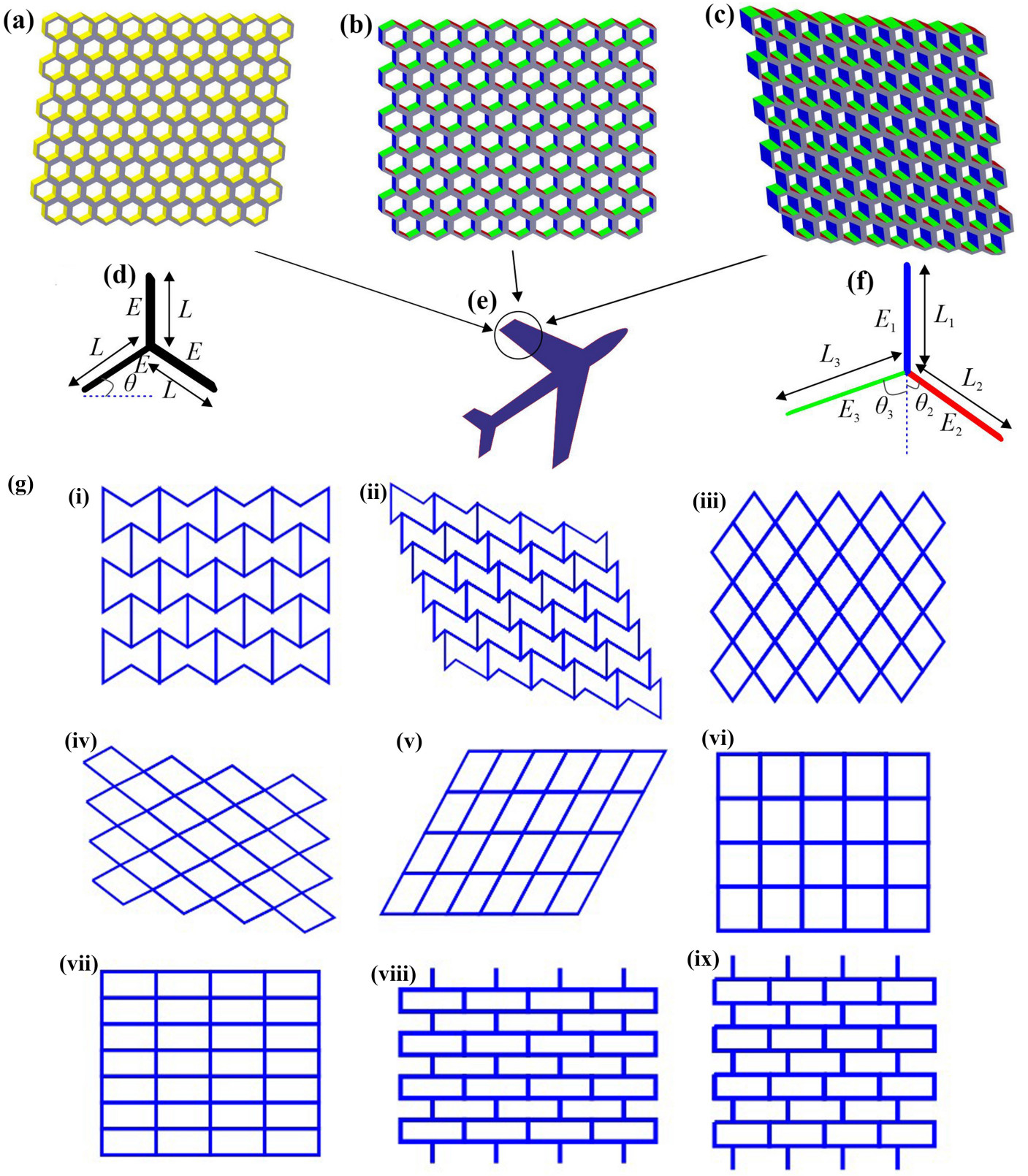

Figure 1: Bottom-up multi-scale approach for asymmetric multimaterial lattices. **(a-b)** Regular mono and multi-material hexagonal lattices with symmetric geometry. **(c)** Asymmetric hexagonal multi-material lattices with different intrinsic materials in the three constituent cell walls. **(d, f)** A symmetric mono-material honeycomb unit cell is shown in (d). The unit cell for multimaterial asymmetric lattices is shown in (f). **(e)** Prospective application of honeycomb lattices in an aircraft following a multi-scale framework (beam-level architecture to unit cell geometries and equivalent metamaterial properties, and subsequently structural applications). **(g)** Lattice derivatives that can be obtained from the generic asymmetric hexagonal lattice shown in subfigure (c), **(i)** Normal auxetic lattice, **(ii)** Asymmetric auxetic lattice, **(iii)** Normal rhombic lattice, **(iv)** Asymmetric rhombic lattice, **(v)** Normal Parallelogram lattice, **(vi)** Normal square lattice, **(vii)** Normal rectangular lattice, **(viii)** Symmetric brick lattice, **(ix)** Asymmetric brick lattice.

2. Derivation of the full constitutive matrices

2.1. Closed-form expressions for elastic moduli C_{12}, C_{22} and C_{32}

A typical unit cell of the proposed asymmetric multimaterial hexagonal honeycombs is shown in Fig. 2(a). In this section, the expressions of three elastic moduli have been derived by keeping one cell wall parallel to the y-axis, as shown in Fig. 2(b) representing the schematic hexagonal geometry with an edge parallel to the y-axis [45, 46]. The considered model has two opposite edges that have the same length and are also parallel. The γ_{12}, γ_{23}, and, γ_{31} represent internal angles between the hexagon edges, as shown in Fig. 2(a).

$$\gamma_{12} + \gamma_{23} + \gamma_{31} = 2\,\pi \tag{1}$$

Here θ_1, θ_2 and θ_3 represent the angle of edges L_1, L_2 and L_3 with the y-axis. For the present case, the angle θ_1 will be zero. Subsequently the θ_2 and θ_3 can be expressed in term of γ_{12} and γ_{13} as,

$$\theta_2 = \pi - \gamma_{12}, \quad \theta_3 = \pi - \gamma_{13} \tag{2}$$

where γ_{12} is the internal angle between constitutive edges L_1 and L_2, and γ_{13} is the internal angle between constitutive edges L_1 and L_3.

The relationship of the relative displacement with axial strain ε_x, ε_y and with the shear strain ε_{xy} can be expressed as

$$\begin{pmatrix} \delta_{ix} \\ \delta_{iy} \end{pmatrix} = \begin{bmatrix} \varepsilon_x & \varepsilon_{xy} + \omega_{xy} \\ \varepsilon_{xy} - \omega_{xy} & \varepsilon_y \end{bmatrix} \begin{pmatrix} L_{ix} \\ L_{iy} \end{pmatrix} \tag{3}$$

In the above Eq. 3, the δ_{ix} and δ_{iy} represent the deflection for a particular cell element, due to applied stress, σ_y in the y direction. L_{ix} and L_{iy}, represent the length of particular a unit cell wall along the x and y-axis, respectively.

The main objective of the study is to obtain the effective in-plane elastic modulus for multi-material asymmetric hexagonal structures with variably-thickened cell walls. Hence, It is considered that the unit cell is heterogeneous in nature and the cell walls are made up of different materials having elastic modulus of E_1, E_2, and E_3 for walls 1, 2 and 3 respectively (refer to Fig. 2(a)). The relation of strains ε_x, ε_y and ε_{xy} with the stresses σ_x, σ_y and τ_{xy} in term of equivalent elastic constitutive elements is given by

$$\begin{pmatrix} \varepsilon_x \\ \varepsilon_y \\ \varepsilon_{xy} \end{pmatrix} = \begin{bmatrix} C_{11} & C_{12} & C_{13} \\ C_{21} & C_{22} & C_{23} \\ C_{31} & C_{32} & C_{33} \end{bmatrix} \begin{pmatrix} \sigma_x \\ \sigma_y \\ \tau_{xy} \end{pmatrix} \tag{4}$$

In present case, stress σ_y is only applied in y-direction, therefore σ_x=τ_{xy}=0. Then from the above Eq. 4,

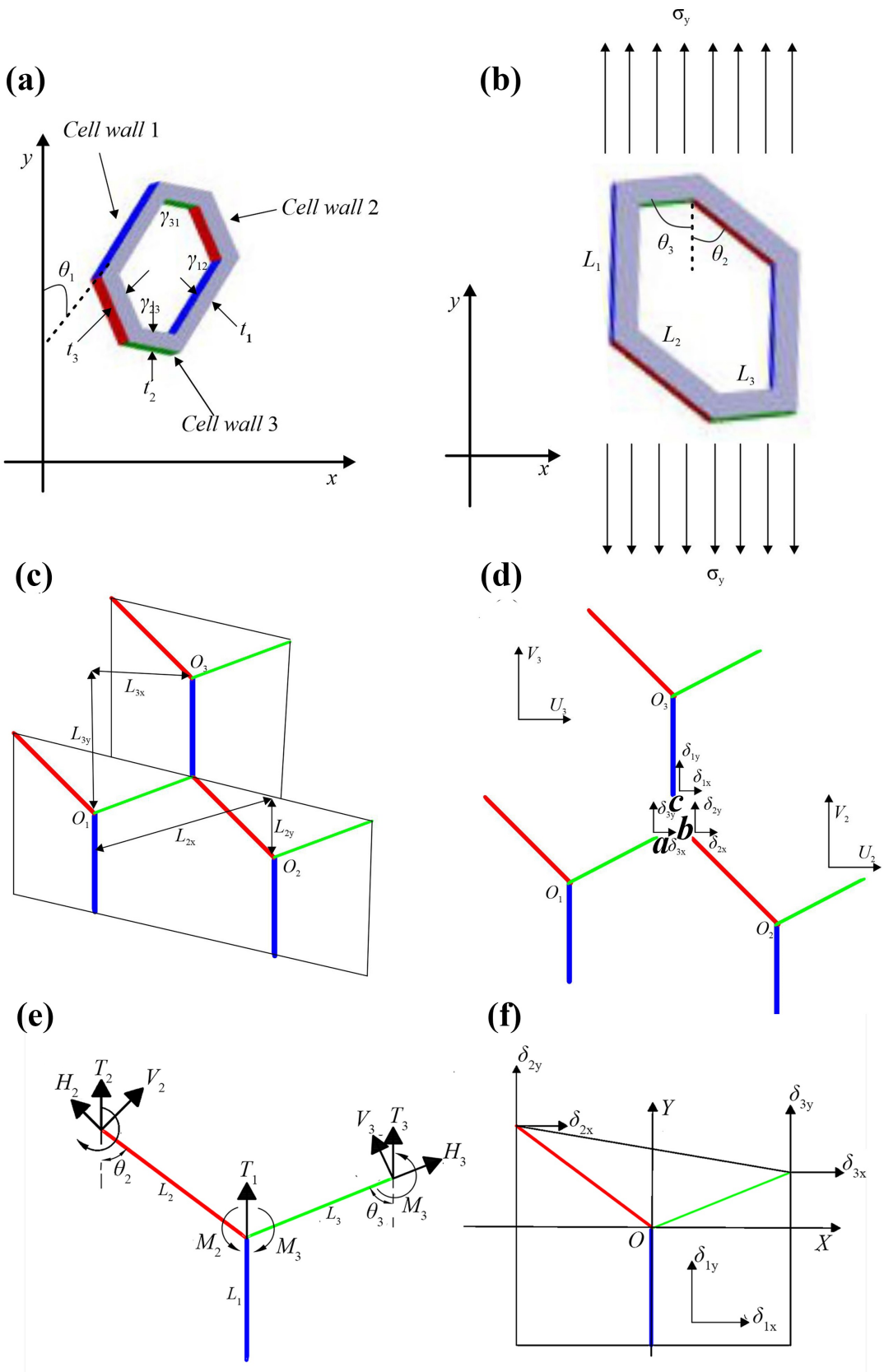

Figure 2: Geometrical details of asymmetric hexagonal honeycombs. **(a)** Unit cell of asymmetric multimaterial hexagonal honeycombs. **(b)** Geometry of hexagonal asymmetric honeycomb unit cell with one edge parallel to y-axis. **(c, d)** Mechanics of multi-material honeycomb cell walls subjected to stress σ_y in y-direction. **(e)** Stress resultants of multi-material honeycomb cell walls subjected to stress σ_y in y-direction. **(f)** Displacements of the cell walls of a unit cell of asymmetric honeycomb lattices.

the expressions for C_{ij} can be obtained.

$$C_{12} = \frac{\varepsilon_x}{\sigma_y}, \qquad C_{22} = \frac{\varepsilon_y}{\sigma_y}, \qquad C_{32} = \frac{\varepsilon_{xy}}{\sigma_y}. \tag{5}$$

For obtaining the values of C_{12}, C_{22} and C_{32}, given in Eq. 5, we need to obtain the values of ε_x, ε_y and ε_{xy} for applied stress σ_y along y-direction. Subsequently, to calculate strains ε_x, ε_y and ε_{xy} the deflections of each constituent element of the unit cell must be obtained first. In the following three sections, we present three different approaches to determining the strain field (ε_x, ε_y and ε_{xy}) in terms of cell wall end deflections (δ_{ix} and δ_{iy}, $i = 1, 2, 3$). While we discuss all three approaches here for a comprehensive understanding, any one of these three approaches can be adopted to establish a relationship between the strain field and cell wall end deflections.

2.1.1. Evaluation of strain field under the application of σ_y

Here we present three different approaches for obtaining strain field under the application of σ_y, among which any one can be adopted for further calculations [45, 46]. It is verified that the results obtained by these three approaches agree well with each other, providing a sense of confidence in the presented analytical framework.

2.1.1.1. Approach 1 for obtaining the strain field

Overaker et al. [67] proposed a novel method to obtain the equivalent strain field that satisfies the displacements of each cell wall. The displacements δ_{ix} and δ_{iy}, which are due to rigid body displacements u_0 and v_0, rigid body rotation ω_{xy} and uniform strain fields ε_x and ε_y, can be expressed as

$$\begin{aligned} \delta_{ix} &= x_i\varepsilon_x + y_i\varepsilon_{xy} + y_i\omega_{xy} + u_0, \\ \delta_{iy} &= y_i\varepsilon_y + x_i\varepsilon_{xy} - x_i\omega_{xy} + v_0. \end{aligned} \tag{6}$$

Here δ_{ix} and δ_{iy} represent the i-th cell wall end deflections with co-ordinates x_i and y_i ($i = 1, 2, 3$). After obtaining deflections along x and y-directions, unknown constants ε_x, ε_y, ε_{xy}, ω_{xy}, u_0 and v_0 can be evaluated by using the Eq. 6. Further, using these obtained strain fields, the equivalent elastic moduli C_{12}, C_{22}, C_{32} can be obtained by using Eq. 5.

2.1.1.2. Approach 2 for obtaining the strain field

The strain field of the honeycomb structure can also be obtained by evaluating relative displacements between the unit cells of the honeycomb. To demonstrate this method more, a part of the honeycomb structure having three unit cells, shown in Fig. 2(c), is considered, which are denoted by unit 1, unit 2 and unit 3. The arrangement of these unit cells is anti-clockwise, and O_1, O_2 and O_3 represent the

cell walls junction of each unit cell. Here U_{21} and V_{21} represent the x-direction and y-direction relative displacement of O_2 with respect to O_1, respectively, as shown in Fig. 2(d). Similarly, U_{31} and V_{31} represent the x-direction and y-direction relative displacement of O_3 with respect to O_1, respectively, as shown in Fig. 2. These relative displacements (U_{21}, V_{21}, and U_{31}, V_{31}) of O_2 and O_3 with respect to O_1 depend upon the strain field caused by the application of stress σ_y in y-direction and given by,

$$\begin{pmatrix} U_{21} \\ V_{21} \\ U_{31} \\ V_{31} \end{pmatrix} = \begin{bmatrix} L_{2x} & 0 & -L_{2y} & -L_{2y} \\ 0 & -L_{2y} & L_{2x} & -L_{2x} \\ L_{3x} & 0 & L_{3y} & L_{3y} \\ 0 & L_{3y} & L_{3x} & L_{3x} \end{bmatrix} \begin{pmatrix} \varepsilon_x \\ \varepsilon_y \\ \varepsilon_{xy} \\ \omega_{xy} \end{pmatrix} \tag{7}$$

Here, L_{2x} and L_{2y} are distances between O_2 and O_1 along x-direction and y-direction, respectively. Similarly, L_{3x} and L_{3y} are distances between O_3 and O_1 along x-direction and y-direction, respectively. These distance constants (L_{2x}, L_{3x}, L_{2y} and L_{3y}) are given by

$$\begin{aligned} L_{2x} &= L_2 sin\theta_2 + L_3 sin\theta_3, \\ L_{2y} &= L_2 cos\theta_2 - L_3 cos\theta_3, \\ L_{3x} &= L_3 sin\theta_3, \\ L_{3y} &= L_1 + L_3 cos\theta_3. \end{aligned} \tag{8}$$

After obtaining, L_{2x}, L_{3x}, L_{2y} and L_{3y}, strain fields ε_x, ε_y, ε_{xy}, ω_{xy} can be represented in terms of L_{2x}, L_{3x}, L_{2y} and L_{3y} by using Eq. 7 as,

$$\begin{aligned} \varepsilon_x &= \frac{L_{3y}U_{21} + L_{2y}U_{31}}{(L_{2y}L_{3x} + L_{2x}L_{3y})}, \\ \varepsilon_y &= \frac{-L_{3x}V_{21} + L_{2x}V_{31}}{(L_{2y}L_{3x} + L_{2x}L_{3y})}, \\ \varepsilon_{xy} &= \frac{-L_{3x}U_{21} + L_{3y}V_{21} + L_{2x}U_{31} + L_{2y}V_{31}}{2(L_{2y}L3x + L_{2x}L_{3y})}, \\ \omega_{xy} &= \frac{L_{3x}U_{21} - L_{3y}V_{21} + L_{2x}U_{31} - L_{2y}V_{31}}{2(L_{2y}L_{3x} + L_{2x}L_{3y})}. \end{aligned} \tag{9}$$

The relative displacements between unit cells can be represented in terms of the relative displacement between junctions and the wall ends of each adjacent unit. To calculate the relative displacements, three points 'a', 'b' and 'c' are considered on unit cells 1, 2 and 3, respectively, as shown in Fig. 2(d). Point 'a' is considered on unit 1 at the end of wall 3 and Point 'b' is considered on unit 2 at the end of wall 2. Similarly, Point 'c' is on unit 3 at the end of wall 1. The relative displacements of point 'a' with respect to O_1 along x direction (U_{a1}) and along y direction (V_{a1}) are equal to cell wall deformation due

to applied stress σ_y in y-direction,

$$\begin{aligned} U_{a1} &= \delta_{3x}, \\ V_{a1} &= \delta_{3y}. \end{aligned} \tag{10}$$

The displacements of point 'b' (U_{b1}, V_{b1}) and point 'c' (U_{c1}, V_{c1}) with respect to point O_1 in the respective x and y-directions can be calculated by adding the respective displacement between the units to the displacements due to the cell wall deformation itself, as presented in Eq.11.

$$\begin{aligned} U_{b1} &= \delta_{2x} + U_{21}, \\ V_{b1} &= \delta_{2y} + V_{21}, \\ U_{c1} &= \delta_{1x} + U_{31}, \\ V_{c1} &= \delta_{1y} + V_{31}. \end{aligned} \tag{11}$$

As shown in Fig. 2(d), the points 'a', 'b' and 'c' are the same point which is located at the same position (at the junction of unit 1, 2 and 3). Hence, the displacements of points 'a', 'b' and 'c' after the deformation will be the same and hold the conditions U_{A1}=U_{B1}=U_{C1} and V_{A1}=V_{B1}=V_{C1}. Based on these conditions, the relative displacements of O_2 (U_{21}, V_{21}) and O_3 (U_{31}, V_{31})) with respect to O_1 along x and y-directions can be expressed as,

$$\begin{aligned} U_{21} &= \delta_{3x} - \delta_{2x}, \\ V_{21} &= \delta_{3y} - \delta_{2y}, \\ U_{31} &= \delta_{3x} - \delta_{1x}, \\ V_{31} &= \delta_{3y} - \delta_{1y}. \end{aligned} \tag{12}$$

Then, strain fields ε_x, ε_y, ε_{xy}, ω_{xy} can be obtained in closed-form by substituting Eq.11 and 12 into Eq. 9.

2.1.1.3. Approach 3 for obtaining the strain field

Here we present another approach of obtaining ε_x, ε_y and ε_{xy} in terms of δ_{ix} and δ_{iy} under applied stress σ_y. Fig. 3(c) and (d) represent unit cells of the considered asymmetric honeycomb lattice. Depending on computational convenience any one form of these two unit cells can be considered with appropriate periodic boundary conditions. The unit cell model of honeycomb lattice, as shown in Fig. 3(d), is considered here to formulate the expressions for the strain field. Strains have been formulated by the calculation of relative displacement of the constitutive cell wall elements, OE, AO, and OD, and which are made of intrinsic materials elastic moduli of E_1, E_2, and E_3 respectively. Lengths of the cell walls have been considered as L_1, L_2, and L_3, respectively.

In the Fig. 3(d), $C'D = CE$. The Y-direction strain can be calculated from the amount of extension

in L_Y length along the Y-direction line FE. $U_{Y\big|_{FE}}$, represents the relative Y-direction displacement of point F with respect to point E.

$$\epsilon_y = \frac{U_{Y\big|_{FE}}}{L_Y}, \tag{13}$$

The value of L_Y in terms of known variables is displayed in Eq.14, and can be calculated using the geometry presented in Fig. 3(d).

$$L_Y = L_1 + \frac{L_2 L_3 sin(\theta_2 + \theta_3)}{L_2 sin\theta_2 + L_3 sin\theta_3} \tag{14}$$

The relative displacement of FE is equal to the sum of the relative displacements of FO and OE, as expressed in Eq.15.

$$U_{Y\big|_{FE}} = U_{Y\big|_{FO}} + U_{Y\big|_{OE}} \tag{15}$$

Since line AD remains straight after deformation, this is represented as in Eq.16.

$$U_{Y\big|_{FO}} = U_{Y\big|_{AO}} \frac{FO}{AD} + U_{Y\big|_{DO}} \frac{FA}{AD} \quad = \frac{\delta_{2y} L_3 sin\theta_3 + \delta_{3y} L_2 sin\theta_2}{L_2 sin\theta_2 + L_3 sin\theta_3}, \tag{16}$$

Considering $U_{Y\big|_{OE}} = -\delta_{1y}$, the strain ϵ_y is provided in expression in Eq. 17.

$$\epsilon_y = \frac{-\delta_{1y} + \dfrac{\delta_{2y} L_3 sin\theta_3 + \delta_{3y} L_2 sin\theta_2}{L_2 sin\theta_2 + L_3 sin\theta_3}}{L_Y} \tag{17}$$

A similar procedure is used to calculate the strain, ε_x in the X-direction, which is dependent on the X-direction deformation of BD as depicted in Fig. 3(d), and the corresponding expression is given in Eq.18..

$$\epsilon_x = \frac{U_{Y\big|_{DB}}}{L_X}, \tag{18}$$

where L_X is the length of the unit cell in the X-direction and is given in terms of known variables in Eq.19.

$$L_X = L_2 sin\theta_2 + L_3 sin\theta_3, \tag{19}$$

The relative displacement of DB is given in the Eq.20, as a sum of the relative displacements of DA and AB.

$$\begin{aligned} U_{X\big|_{DB}} &= U_{X\big|_{DA}} + U_{X\big|_{AB}} \\ U_{X\big|_{DA=\delta_{3x}-\delta_{2x}}} & \end{aligned} \tag{20}$$

For the calculation of relative distance AB, as shown in Eq.21, the displacement of each point along line AC from point A to point C is linearly distributed. The deformation should leave the line AC straight,

so the displacement of point B is provided below.

$$\begin{aligned} U_{X\big|_{AB}} &= U_{X\big|_{AC}} \frac{AB}{AC} = U_{X\big|_{AC}} \frac{L_2 cos\theta_2 - L_3 cos\theta_3}{L_Y} \\ U_{X\big|_{AC}} &= U_{X\big|_{AO}} + U_{X\big|_{OE}} + U_{X\big|_{EC}} = \delta_{2x} + 0 + U_{X\big|_{EC}} \end{aligned} \tag{21}$$

The points C' and D in Fig. 3(d) are analogous to C and E, respectively.

$$\begin{aligned} U_{X\big|_{EC}} &= U_{X\big|_{DC'}} \\ U_{X\big|_{DC'}} &= U_{X\big|_{DA}} \frac{DC'}{AD} = (\delta_{3x} - \delta_{2x}) \frac{L_2 sin\theta_2}{L_2 sin\theta_2 + L_3 sin\theta_3} \\ U_{X\big|_{DB}} &= \delta_{3x} - \delta_{2x} + \left(\frac{\delta_{2x} L_3 sin\theta_3 + \delta_{3x} L_2 sin\theta_2}{L_2 sin\theta_2 + L_3 sin\theta_3} \right) \left(\frac{L_2 cos\theta_2 - L_3 cos\theta_3}{L_X L_Y} \right) \end{aligned} \tag{22}$$

Finally, the expression of strain, $epsilon_x$, is given in Eq.23.

$$\epsilon_x = \frac{\delta_{3x} - \delta_{2x}}{L_X} + \left(\frac{\delta_{2x} L_3 sin\theta_3 + \delta_{3x} L_2 sin\theta_2}{L_2 sin\theta_2 + L_3 sin\theta_3} \right) \left(\frac{L_2 cos\theta_2 - L_3 cos\theta_3}{L_X L_Y} \right) \tag{23}$$

The shear strain, ϵ_{xy}, can be calculated using the expressions in Eq.24.

$$\epsilon_{xy} = \frac{1}{2} \left(\frac{U_{X\big|_{FE}}}{L_Y} + \frac{U_{Y\big|_{DB}}}{L_X} \right) \tag{24}$$

The relative displacement of FE is yielded as the sum of relative displacements of FO and OE, as shown in Eq.25.

$$\begin{aligned} U_{X\big|_{FE}} &= U_{X\big|_{FO}} + U_{X\big|_{OE}} = U_{X\big|_{AO}} \frac{AF}{AD} + U_{X\big|_{DO}} \frac{DF}{AD} + 0 \\ &= \delta_{2x} \left(\frac{L_3 sin\theta_3}{L_2 sin\theta_2 + L_3 sin\theta_3} \right) + \delta_{3x} \left(\frac{L_2 sin\theta_2}{L_2 sin\theta_2 + L_3 sin\theta_3} \right) \end{aligned} \tag{25}$$

The term $U_{Y\big|_{DB}}$ shown on the right-hand side of Eq.24 can now be represented as shown in Eq.26.

$$\begin{aligned} U_{Y\big|_{DB}} &= U_{Y\big|_{DA}} + U_{Y\big|_{AB}} = (\delta_{3y} - \delta_{2y}) + U_{Y\big|_{AC}} \frac{AB}{AC} \\ where, \frac{AB}{AC} &= \frac{L_2 cos\theta_2 - L_3 cos\theta_3}{L_Y} \end{aligned} \tag{26}$$

The expression of $U_{Y\big|_{AC}}$ is given below.

$$\begin{aligned} U_{Y\big|_{AC}} &= U_{Y\big|_{AO}} + U_{Y\big|_{OE+U_{Y\big|_{EC}}}} = (\delta_{2y} - \delta_{1y}) + U_{Y\big|_{DC'}} \\ &= \delta_{2y} - \delta_{1y} + U_{Y\big|_{DA}} \frac{DC'}{AO} = \delta_{2y} - \delta_{1y} + (\delta_{3y} - \delta_{2y}) \frac{L_2 sin\theta_2}{L_X} \\ &= -\delta_{1y} + \frac{\delta_{2y} L_3 sin\theta_3 + \delta_{3y} L_2 sin\theta_2}{L_2 sin\theta_2 + L_3 sin\theta_3} \end{aligned} \tag{27}$$

Eq. 28 provides the expressions for shear strain, ϵ_{xy}, in terms of known variables.

$$\begin{aligned}\epsilon_{xy} = &\frac{1}{2}\left(\frac{\delta_{2x}L_3 sin\theta_3 + \delta_{3x}L_2 sin\theta_2}{L_Y(L_2 sin\theta_2 + L_3 sin\theta_3)}\right) \\ &+ \frac{1}{2}\left(\frac{\delta_{3y} - \delta_{2y}}{L_X} + \frac{L_2 cos\theta_2 - L_3 cos\theta_3}{L_X L_Y}\left(-\delta_{1y} + \frac{\delta_{2y}L_3 sin\theta_3 + \delta_{3y}L_2 sin\theta_2}{L_2 sin\theta_2 + L_3 sin\theta_3}\right)\right)\end{aligned} \tag{28}$$

Up to this point, we have formulated the expressions for ε_x, ε_y, and ε_{xy} in terms of δ_{ix} and δ_{iy}, the derivation of which are provided in the next section.

2.1.2. Cell wall end deflections under the application of σ_y

After obtaining the strain field, as discussed in the preceding section following three different approaches, equivalent elastic modulus C_{12}, C_{22} and C_{32} can be calculated from Eq. 5. But for obtaining ε_x, ε_y and ε_{xy}, the cell wall end deflections need to be evaluated. In this section, we concentrate on evaluating δ_{ix} and δ_{iy}, which can directly be used in any one of the three approaches. Further, it may be noted that the effects of multi-material unit cells and variably thickened cell walls would be incorporated here.

The closed-form expressions for force, moment, and displacement are derived here under the application of σ_y. The schematic diagram of forces and moments on each cell wall due to applied stress σ_y in y-direction is shown in Fig. 2(e). The expression of acting forces can be obtained from the equilibrium condition of forces.

$$\begin{aligned}T_1 &= \sigma_y h(L_3 sin\theta_3 + L_2 sin\theta_2), \\ T_2 &= \sigma_y h L_3 sin\theta_3, \\ T_3 &= \sigma_y h L_2 sin\theta_2,\end{aligned} \tag{29}$$

Here, T_1, T_2 and T_3 represent the acting forces along the y-direction at cell wall 1, 2 and 3, respectively. From the above expressions of Eq. 29, it is clear that $T_1 = T_2 + T_3$. The moments that are produced due to these forces T_i acting on each wall can be expressed as shown in Eq.30.

$$\begin{aligned}M_1 &= 0, \\ M_2 &= T_2\frac{1}{2}L_2 sin\theta_2 = \frac{1}{2}\sigma_y h L_2 sin\theta_2 L_3 sin\theta_3, \\ M_3 &= T_3\frac{1}{2}L_3 sin\theta_3 = \frac{1}{2}\sigma_y h L_2 sin\theta_2 L_3 sin\theta_3\end{aligned} \tag{30}$$

where $M_2 = M_3$. M_1, M_2 and M_3 represent the resulting moments on cell walls 1, 2 and 3, respectively.

The closed-form expressions are derived now for the displacements of each cell wall along the x and y directions. It is considered that the thickness of the cell walls is higher at the ends and comparatively less at the center of the wall element (i.e. variably thickened beams), as shown in Fig. 3(a, b). Note

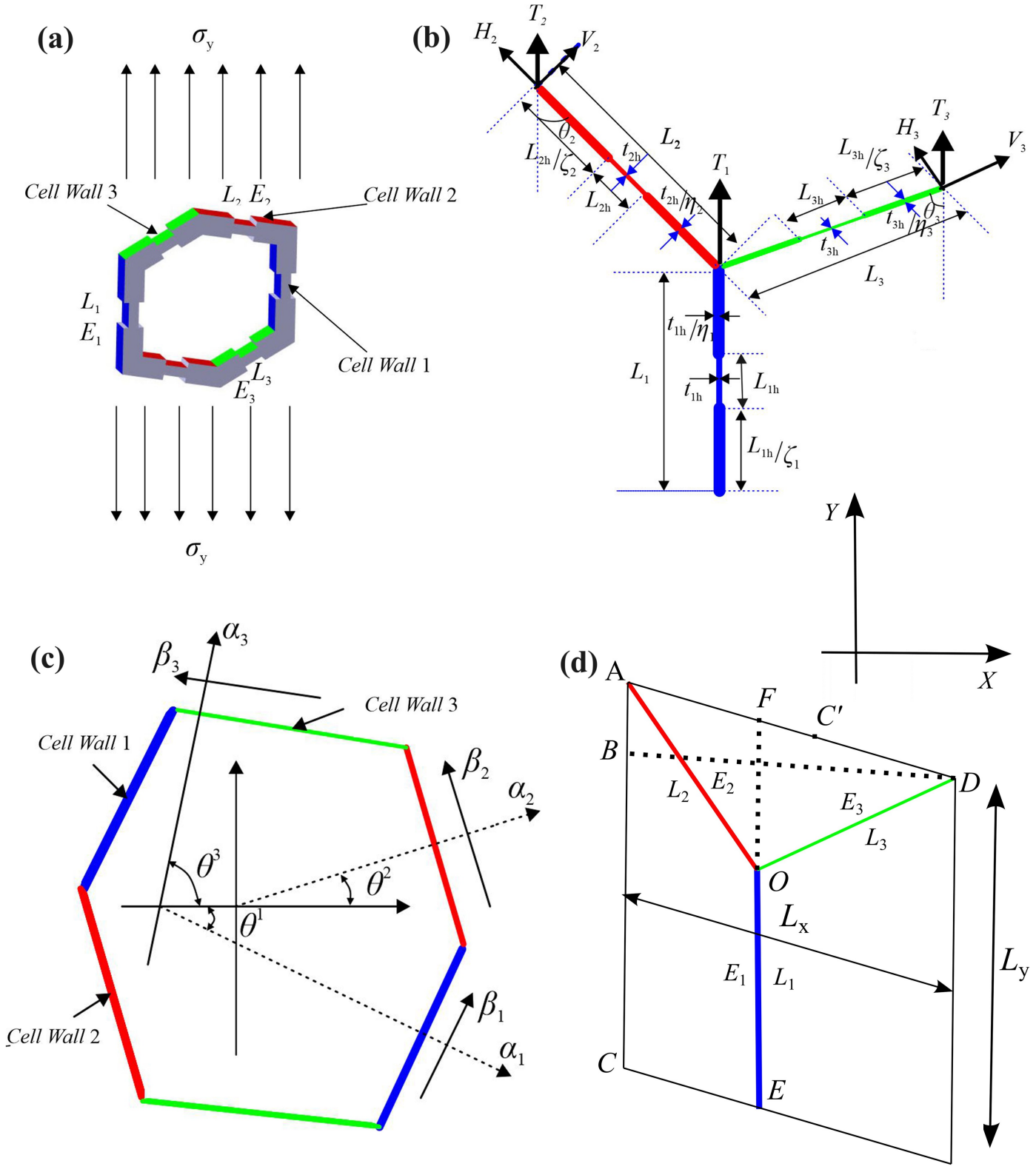

Figure 3: Beam-level variably-thickened architecture in asymmetric multimaterial lattices. **(a)** Geometry of asymmetric honeycomb hexagonal unit cell with one edge parallel to Y-axis, subjected to stress σ_y. **(b)** Geometric details and stress resultants in a variably-thickened asymmetric unit cell. **(c)** α_i, β_i coordinates for co-ordinate transformation. **(d)** Asymmetric unit cell for analyzing the strain field following Approach 3.

here that we have considered the variation of thickness along the beam lengths keeping the bending moments in mind for a both-end rotationally restrained support condition. Though we have taken the

stepped variation of thickness in each of the beams, continuous variation can also be considered based on the currently proposed approach (the final expressions for cell wall deflections need to be derived accordingly).

In a variably-thickened wall, η_i and ζ_i are the thickness ratio parameter and span ratio parameter, respectively. Here, ζ_i represents the ratio of the middle part length having less thickness to the end part's length with higher thickness, as shown in Fig 3(b). Similarly, η_i represents the ratio of the middle part thickness to the end part thickness, as shown in Fig 3(b).

Based on energy method [37], the axial deflection of cell wall 1 can be expressed as

$$\delta_1\big|_{axial} = \frac{\partial U}{\partial T_1}, U = \int_0^{L_1} \frac{-{T_1}^2}{2E_1A_1}dx \tag{31}$$

Now, the closed-form expression for axial deflection of cell wall 1 having different thickness segments can be expressed as,

$$\begin{aligned} &\frac{-T_1}{E_1h_1}\int_0^{L_1}\frac{1}{t_{1x}}dx = \frac{-T_1}{E_1h_1}\left(\int_0^{\frac{L_{1h}}{\zeta_1}}\frac{\eta_1}{t_{1h}}dx + \int_{\frac{L_{1h}}{\zeta_1}}^{L_{1h}+\frac{L_{1h}}{\zeta_1}}\frac{1}{t_{1h}}dx + \int_{L_{1h}+\frac{L_{1h}}{\zeta_1}}^{L_{1h}+2\frac{L_{1h}}{\zeta_1}}\frac{1}{t_{1h}}dx\right), \\ &\delta_{1axial} = \frac{-T_1L_1}{E_1h_1t_{1h}}\left(\frac{2\eta_1+\zeta_1}{2+\zeta_1}\right) \end{aligned} \tag{32}$$

Further, the axial deflection cell wall 1 can be split into its components along the x and y direction as,

$$\begin{aligned} \delta_{1x}\big|_{axial} &= 0, \\ \delta_{1y}\big|_{axial} &= \frac{-T_1L_1}{E_1h_1t_{1h}}\left(\frac{2\eta_1+\zeta_1}{2+\zeta_1}\right). \end{aligned} \tag{33}$$

It is worth noting that deflection of cell wall 1 due to bending and shear will be zero because no bending moment and shear force are acting on cell wall 1.

Similarly, using energy method the deflections of cell wall 2 and 3 can be evaluated in a closed-form manner. Due to the presence of axial force, bending moment and shear force on cell wall 2 and 3, the overall deflection consists of deformation due to axial, bending and shear force as,

$$\begin{aligned} \delta_2\big|_{total} &= \delta_{2axial} + \delta_{2bending} + \delta_{2shear}, \\ \delta_3\big|_{total} &= \delta_{3axial} + \delta_{3bending} + \delta_{3shear}. \end{aligned} \tag{34}$$

By employing the energy method, axial deflection of cell wall 2 can be expressed as

$$\delta_{2axial} = \frac{\partial U}{\partial H_2}, U = \int_0^{L_2} \frac{{H_2}^2}{2E_2A_2}dx,$$

$$U = \frac{H_2^2}{2E_2h_2}\int_0^{L_2}\frac{1}{t_{2x}}dx = \frac{H_2^2}{2E_2h_2}\left(\int_0^{\frac{L_{2h}}{\zeta_2}}\frac{\eta_2}{t_{2h}}dx + \int_{\frac{L_{2h}}{\zeta_2}}^{L_{2h}+\frac{L_{2h}}{\zeta_2}}\frac{1}{t_{2h}}dx + \int_{L_{2h}+\frac{L_{2h}}{\zeta_2}}^{L_{2h}+2\frac{L_{2h}}{\zeta_2}}\frac{\eta_2}{t_{2h}}dx\right), \tag{35}$$

$$U = \frac{H_2^2L_2}{2E_2h_2t_{2h}}\left(\frac{2\eta_2+\zeta_2}{2+\zeta_2}\right)$$

where, $H_2 = T_2\cos\theta_2$. Hence,

$$\begin{aligned} U &= \frac{(T_2\cos\theta_2)^2L_2}{2E_2h_2t_{2h}}\left(\frac{2\eta_2+\zeta_2}{2+\zeta_2}\right), \\ \delta_{2|axial} &= \frac{\partial U}{\partial H_2} = \frac{T_2\cos\theta_2L_2}{E_2h_2t_{2h}}\left(\frac{2\eta_2+\zeta_2}{2+\zeta_2}\right) \end{aligned} \tag{36}$$

The axial deflection of cell wall 2, given in Eq. 36, can be split into its component along the x and y direction as

$$\begin{aligned} \delta_{2x}\big|_{axial} &= -\frac{T_2L_2\cos\theta_2\sin\theta_2}{E_2h_2t_{2h}}\left(\frac{2\eta_2+\zeta_2}{2+\zeta_2}\right), \\ \delta_{2y}\big|_{axial} &= \frac{T_2L_2\cos^2\theta_2}{E_2h_2t_{2h}}\left(\frac{2\eta_2+\zeta_2}{2+\zeta_2}\right), \\ &\text{where, } L_2 = L_{2h} + \frac{L_{2h}}{\zeta_2}. \end{aligned} \tag{37}$$

The energy method can also be utilized for driving closed-from expression of bending deflection for cell elements. Based on the energy method, the bending deflection of cell wall 2 can be expressed as,

$$\delta_2\big|_{bending} = \frac{\partial U}{\partial V_2}, U = \int_0^{L_2}\frac{{M_2}^2}{2E_2I_2}dx,$$

$$\text{where,} \quad M_2 = \frac{1}{2}T_2\sin\theta_2 x, \quad \text{and} \quad V_2 = T_2\sin\theta_2,$$

$$U = \frac{T_2^2\sin^2\theta_2}{16E_2}\int_0^{L_2}\frac{x^2}{I_{2x}}dx = \frac{T_2^2\sin^2\theta_2}{16E_2}\left(\int_0^{\frac{L_{2h}}{\zeta_2}}\frac{\eta_2^3x^2}{I_2}dx + \int_{\frac{L_{2h}}{\zeta_2}}^{L_{2h}+\frac{L_{2h}}{\zeta_2}}\frac{x^2}{I_2}dx + \int_{L_{2h}+\frac{L_{2h}}{\zeta_2}}^{L_{2h}+2\frac{L_{2h}}{\zeta_2}}\frac{\eta_2^3x^2}{I_2}dx\right), \tag{38}$$

$$U = \frac{T_2^2\sin^2\theta_2}{2E_2h_2}\left(\frac{L_2^3}{t_{2h}^3}\right)\left(\frac{8\eta_2^3+9\eta_2^3\zeta_2+3\eta_2^3\zeta_2^2+\zeta_2^3+3\zeta_2^2+3\zeta_2}{(2+\zeta_2)^3}\right),$$

$$\delta_2\big|_{bending} = \frac{\partial U}{\partial V_2} = \frac{T_2\sin\theta_2}{E_2h_2}\left(\frac{L_2^3}{t_{2h}^3}\right)\left(\frac{8\eta_2^3+9\eta_2^3\zeta_2+3\eta_2^3\zeta_2^2+\zeta_2^3+3\zeta_2^2+3\zeta_2}{(2+\zeta_2)^3}\right),$$

The bending deflections along x and y directions can be obtained as,

$$\begin{aligned} \delta_{2y}\big|_{bending} &= \frac{T_2\sin^2\theta_2}{E_2h_2}\left(\frac{L_2^3}{t_{2h}^3}\right)\left(\frac{8\eta_2^3+9\eta_2^3\zeta_2+3\eta_2^3\zeta_2^2+\zeta_2^3+3\zeta_2^2+3\zeta_2}{(2+\zeta_2)^3}\right), \\ \delta_{2x}\big|_{bending} &= \frac{T_2\sin\theta_2\cos\theta_2}{E_2h_2}\left(\frac{L_2^3}{t_{2h}^3}\right)\left(\frac{8\eta_2^3+9\eta_2^3\zeta_2+3\eta_2^3\zeta_2^2+\zeta_2^3+3\zeta_2^2+3\zeta_2}{(2+\zeta_2)^3}\right), \end{aligned} \tag{39}$$

The energy method is also utilized to obtain the deflection of cell wall 2 due to shear force V_2.

$$\delta_2\big|_{shear} = \frac{\partial U}{\partial V_2}, \quad \text{where} \quad U = \int_0^{L_2} \frac{{V_2}^2}{2G_2A_2}dx,$$

$$U = \frac{T_2^2\sin^2\theta_2}{G_2h_2}\int_0^{L_2}\frac{1}{t_{2x}}dx = \frac{T_2^2\sin^2\theta_2}{G_2h_2}\left(\int_0^{\frac{L_{2h}}{\zeta_2}}\frac{\eta_2}{t_{2h}}dx + \int_{\frac{L_{2h}}{\zeta_2}}^{L_{2h}+\frac{L_{2h}}{\zeta_2}}\frac{1}{t_{2h}}dx + \int_{L_{2h}+\frac{L_{2h}}{\zeta_2}}^{L_{2h}+2\frac{L_{2h}}{\zeta_2}}\frac{\eta_2}{t_{2h}}dx\right), \quad (40)$$

$$\delta_2\big|_{shear} = \frac{T_2L_2\sin\theta_2}{G_2h_2t_{2h}}\left(\frac{2\eta_2+\zeta_2}{2+\zeta_2}\right), \qquad \text{where}, V_2 = T_2\sin\theta_2, \quad G_2 = \frac{E_2}{2(1+\nu_2)}$$

Now shear deflection can be also split into its y and x direction components as,

$$\begin{aligned}\delta_{2y}\big|_{shear} &= \frac{T_2L_2\sin^2\theta_2 2(1+\nu_2)}{E_2h_2t_{2h}}\left(\frac{2\eta_2+\zeta_2}{2+\zeta_2}\right),\\ \delta_{2x}\big|_{shear} &= \frac{T_2L_2\sin\theta_2\cos\theta_2 2(1+\nu_2)}{E_2h_2t_{2h}}\left(\frac{2\eta_2+\zeta_2}{2+\zeta_2}\right),\end{aligned} \quad (41)$$

In a similar way, we would calculate the deflection for the third cell element. So, the final formulation for the deflections in x and y directions for the element 3 is given below in Eq. 42.

$$\begin{aligned}\delta_{3x}\big|_{axial} &= \frac{T_3L_3\cos\theta_3\sin\theta_3}{E_3h_3t_{3h}}\left(\frac{2\eta_3+\zeta_3}{2+\zeta_3}\right),\\ \delta_{3y}\big|_{axial} &= \frac{T_3L_3\cos^2\theta_3}{E_3h_3t_{3h}}\left(\frac{2\eta_3+\zeta_3}{2+\zeta_3}\right),\\ where, L_3 &= L_{3h}+\frac{L_{3h}}{\zeta_3}.\\ \delta_{3y}\big|_{bending} &= \frac{T_3\sin^2\theta_3}{E_3h_3}\left(\frac{L_3^3}{t_{3h}^3}\right)\left(\frac{8\eta_3^3+9\eta_3^3\zeta_3+3\eta_3^3\zeta_3^2+\zeta_3^3+3\zeta_3^2+3\zeta_3}{(2+\zeta_3)^3}\right),\\ \delta_{3x}\big|_{bending} &= \frac{-T_3\sin\theta_3\cos\theta_3}{E_3h_3}\left(\frac{L_3^3}{t_{3h}^3}\right)\left(\frac{8\eta_3^3+9\eta_3^3\zeta_3+3\eta_3^3\zeta_3^2+\zeta_3^3+3\zeta_3^2+3\zeta_3}{(2+\zeta_3)^3}\right),\\ \delta_{3y}\big|_{shear} &= \frac{T_3L_3\sin^2\theta_3 2(1+\nu_3)}{E_3h_3t_{3h}}\left(\frac{2\eta_3+\zeta_3}{2+\zeta_3}\right),\\ \delta_{3x}\big|_{shear} &= \frac{-T_3L_3\sin\theta_3\cos\theta_3 2(1+\nu_3)}{E_3h_3t_{3h}}\left(\frac{2\eta_3+\zeta_3}{2+\zeta_3}\right),\\ \text{where}, G_3 &= \frac{E_3}{2(1+\nu_3)}\end{aligned} \quad (42)$$

The total deflections of unit cell walls 1, 2 and 3 along the x-direction due to acting axial, bending

and shear forces are given as,

$$
\begin{aligned}
\delta_{1x}\big|_{total} &= 0, \\
\delta_{2x}\big|_{total} &= -\frac{T_2 L_2 \cos\theta_2 \sin\theta_2}{E_2 h_2 t_{2h}} \left(\frac{2\eta_2 + \zeta_2}{2 + \zeta_2}\right) \\
&\quad + \frac{T_2 \sin\theta_2 \cos\theta_2}{E_2 h_2} \left(\frac{L_2^3}{t_{2h}^3}\right) \left(\frac{8\eta_2^3 + 9\eta_2^3\zeta_2 + 3\eta_2^3\zeta_2^2 + \zeta_2^3 + 3\zeta_2^2 + 3\zeta_2}{(2+\zeta_2)^3}\right) \\
&\quad + \frac{T_2 L_2 \sin\theta_2 \cos\theta_2 2(1+\nu_2)}{E_2 h_2 t_{2h}} \left(\frac{2\eta_2 + \zeta_2}{2 + \zeta_2}\right), \\
\delta_{3x}\big|_{total} &= \frac{T_3 L_3 \cos\theta_3 \sin\theta_3}{E_3 h_3 t_{3h}} \left(\frac{2\eta_3 + \zeta_3}{2 + \zeta_3}\right) \\
&\quad - \frac{T_3 \sin\theta_3 \cos\theta_3}{E_3 h_3} \left(\frac{L_3^3}{t_{3h}^3}\right) \left(\frac{8\eta_3^3 + 9\eta_3^3\zeta_3 + 3\eta_3^3\zeta_3^2 + \zeta_3^3 + 3\zeta_3^2 + 3\zeta_3}{(2+\zeta_3)^3}\right) \\
&\quad - \frac{T_3 L_3 \sin\theta_3 \cos\theta_3 2(1+\nu_3)}{E_3 h_3 t_{3h}} \left(\frac{2\eta_3 + \zeta_3}{2 + \zeta_3}\right)
\end{aligned} \tag{43}
$$

Similarly, the total deflections of unit cell walls 1, 2 and 3 along the y-direction due to acting axial, bending and shear forces are given as,

$$
\begin{aligned}
\delta_{1y}\big|_{total} &= -\frac{T_1 L_1}{E_1 h_1 t_{1h}} \left(\frac{2\eta_1 + \zeta_1}{2 + \zeta_1}\right), \\
\delta_{2y}\big|_{total} &= \frac{T_2 L_2 \cos^2\theta_2}{E_2 h_2 t_{2h}} \left(\frac{2\eta_2 + \zeta_2}{2 + \zeta_2}\right) \\
&\quad + \frac{T_2 \sin^2\theta_2}{E_2 h_2} \left(\frac{L_2^3}{t_{2h}^3}\right) \left(\frac{8\eta_2^3 + 9\eta_2^3\zeta_2 + 3\eta_2^3\zeta_2^2 + \zeta_2^3 + 3\zeta_2^2 + 3\zeta_2}{(2+\zeta_2)^3}\right) \\
&\quad + \frac{T_3 L_3 \sin^2\theta_3 2(1+\nu_3)}{E_3 h_3 t_{3h}} \left(\frac{2\eta_3 + \zeta_3}{2 + \zeta_3}\right), \\
\delta_{3y}\big|_{total} &= \frac{T_3 L_3 \cos^2\theta_3}{E_3 h_3 t_{3h}} \left(\frac{2\eta_3 + \zeta_3}{2 + \zeta_3}\right) \\
&\quad + \frac{T_3 \sin\theta_3 \cos\theta_3}{E_3 h_3} \left(\frac{L_3^3}{t_{3h}^3}\right) \left(\frac{8\eta_3^3 + 9\eta_3^3\zeta_3 + 3\eta_3^3\zeta_3^2 + \zeta_3^3 + 3\zeta_3^2 + 3\zeta_3}{(2+\zeta_3)^3}\right) \\
&\quad + \frac{T_3 L_3 \sin^2\theta_3 2(1+\nu_3)}{E_3 h_3 t_{3h}} \left(\frac{2\eta_3 + \zeta_3}{2 + \zeta_3}\right)
\end{aligned} \tag{44}
$$

2.1.2.1. Special case 1: Multimaterial asymmetric honeycombs with constant cell wall thickness

For an asymmetric multi-material honeycomb structure with a constant thickness along each constitutive cell wall the value of η_i and ζ_i, (i=1, 2 and 3) are equal to unity (η_i=ζ_i = 1). Hence, the expression of deflections of each cell wall along x-direction for the asymmetric multi-material honeycomb structure

with constant thickness reduces to the following form,

$$\begin{aligned}
\delta_{1x} &= 0, \\
\delta_{2x} &= \frac{T_2 sin\theta_2 cos\theta_2}{E_2 h}\left(\frac{L_2}{t_2}\right)^3 + 2(1+\nu_2)\frac{T_2 L_2 sin\theta_2 cos\theta_2}{kE_2 h t_2} - \frac{L_2 T_2 cos\theta_2 sin\theta_2}{E_2 h t_2}, \\
\delta_{3x} &= -\frac{T_3 sin\theta_3 cos\theta_3}{E_3 h}\left(\frac{L_3}{t_3}\right)^3 - 2(1+\nu_3)\frac{T_3 L_3 sin\theta_3 cos\theta_3}{kE_3 h t_3} + \frac{L_3 T_3 cos\theta_3 sin\theta_3}{E_3 h t_3}
\end{aligned} \tag{45}$$

Similarly, the expression of deflections of each cell wall along y-direction for the asymmetric multi-material honeycomb structure with constant thickness reduces to,

$$\begin{aligned}
\delta_{1y} &= -\frac{L_1 T_1}{E_1 h T_1}, \\
\delta_{2y} &= -\frac{T_2 sin^2\theta_2}{E_2 h}\left(\frac{L_2}{t_2}\right)^3 + 2(1+\nu_2)\frac{T_2 L_2 cos^2\theta_2}{E_2 h t_2} + \frac{L_2 T_2 cos^2\theta_2}{E_2 h t_2}, \\
\delta_{3y} &= \frac{T_3 sin^2\theta_3}{E_3 h}\left(\frac{L_3}{t_3}\right)^3 + 2(1+\nu_3)\frac{T_3 L_3 sin^2\theta_3}{kE_3 h t_3} + \frac{L_3 T_3 cos^2\theta_3}{E_3 h t_3}
\end{aligned} \tag{46}$$

2.1.2.2. Special case 2: Monomaterial asymmetric honeycombs with constant cell wall thickness

If the asymmetric hexagonal honeycomb structure is of mono-material (along with having constant thickness), i.e. $E_1 = E_2 = E_3 = E$, then the above expression of displacements for x and y direction further reduces to,

$$\begin{aligned}
\delta_{1x} &= 0, \\
\delta_{2x} &= \frac{T_2 sin\theta_2 cos\theta_2}{Eh}\left(\frac{L_2}{t_2}\right)^3 + 2(1+\nu)\frac{T_2 L_2 sin\theta_2 cos\theta_2}{kEht_2} - \frac{L_2 T_2 cos\theta_2 sin\theta_2}{Eht_2}, \\
\delta_{3x} &= -\frac{T_3 sin\theta_3 cos\theta_3}{Eh}\left(\frac{L_3}{t_3}\right)^3 - 2(1+\nu)\frac{T_3 L_3 sin\theta_3 cos\theta_3}{kEht_3} + \frac{L_3 T_3 cos\theta_3 sin\theta_3}{Eht_3}, \\
\delta_{1y} &= -\frac{L_1 T_1}{Eht_1}, \\
\delta_{2y} &= -\frac{T_2 sin^2\theta_2}{Eh}\left(\frac{L_2}{t_2}\right)^3 + 2(1+\nu)\frac{T_2 L_2 cos^2\theta_2}{Eht_2} + \frac{L_2 T_2 cos^2\theta_2}{Eht_2}, \\
\delta_{3y} &= \frac{T_3 sin^2\theta_3}{Eh}\left(\frac{L_3}{t_3}\right)^3 + 2(1+\nu)\frac{T_3 L_3 sin^2\theta_3}{kEht_3} + \frac{L_3 T_3 cos^2\theta_3}{Eht_3}
\end{aligned} \tag{47}$$

Note that the above case is reported in literature [61], and the expressions presented here agree well with such derivations. This provides an exact analytical validation of the current derivations.

2.1.2.3. Special case 3: Multimaterial symmetric honeycombs with constant cell wall thickness

If we further apply the condition for multi-material symmetric hexagonal structure ($\theta_2 = \theta_3 = \theta$), then we can obtain the expressions for deflection of cell wall 2 and 3 under only bending deformation, similar

to the case of Mukhopadhyay et al. [60].

$$\begin{aligned} \delta_2 &= \frac{T_2 L_2^3 \sin\theta}{12 E_2 I} \\ \delta_3 &= \frac{T_3 L_3^3 \sin\theta}{12 E_3 I} \end{aligned} \tag{48}$$

where, $I = \dfrac{ht^3}{12}$. Though we have neglected the effect of axial and shear deformations in the above equations for comparison with literature [60], these effects can be readily incorporated for multimaterial symmetric honeycombs with constant cell wall thickness.

2.1.2.4. Special case 4: Monomaterial symmetric honeycombs with constant cell wall thickness

For mono-material (E_1= E_2= E_3= E) symmetric hexagonal structures (L_2= L_3= L and T_2= T_3= T), the deflection of cell wall 2 and 3 is given by

$$\begin{aligned} \delta_2 &= \frac{T_2 L^3 \sin\theta}{12 E I} \\ \delta_3 &= \frac{T_3 L^3 \sin\theta}{12 E I} \end{aligned} \tag{49}$$

Though we have neglected the effect of axial and shear deformations in the above equations for comparison with literature [37], these effects can be readily incorporated for monomaterial symmetric honeycombs with constant cell wall thickness.

2.2. Evaluation of full elastic modulus matrix

In the previous section, the method to obtain three elastic moduli C_{12}, C_{22} and C_{32} in closed-form is proposed for muti-material variably-thickened asymmetric honeycombs having hexagon cells with cell wall 1 parallel to the y-axis. But, all nine components of the constitutive matrix, mentioned in Eq.4, must be known to model the overall elastic characteristics of such a honeycomb. In this section, other remaining unknown elastic moduli (C_{11}, C_{13} and C_{33}) are determined in closed-form by utilizing the known elastic moduli C_{12}, C_{22} and C_{32} based on co-ordinate transformation [45, 46].

In Fig. 3(c), α_1 and β_1 represent the coordinate axes for the cell wall 1. Similarly, (α_2, β_2) and (α_3,β_3) represent the coordinate axes for the cell wall 2 and cell wall 3, respectively. Using these coordinates, equivalent elastic modulus can be calculated for all the formed coordinates separately. For such calculations, the (x, y) coordinate axes are transformed to (α, β) coordinate axes by keeping β axis parallel to the cell wall. Therefore, C'_{12},C'_{22}, and C'_{32} in (α_1, β_1) coordinate system, C''_{12}, C''_{22}, and C''_{32} in (α_2, β_2) coordinate system and C'''_{12}, C'''_{22}, and C'''_{32} in (α_3, β_3) coordinate system can be found by coordinate transformation (the upper subscripts in C_{ij} represents a unit cell number). Here, θ^1 is

angle between the coordinate axes (x, y) and (α_1, β_1), as shown in Fig. 3(c). Similarly, θ^2 and θ^3 are angles between the coordinate axes (x, y) with (α_2, β_3) and (α_3, β_3), respectively. In (α_1, β_1) coordinate system θ^1=θ_1, whereas θ^2= θ_1+(π-γ_{12}) for the (α_2, β_2) coordinate system, and θ^3= θ_1+(π-γ_{12})+(π-γ_{23}) for the (α_3, β_3) coordinate system. The transformation of stress and strain from the (x, y) coordinate system to the (α_1, β_1) coordinate system leads to the following equation,

$$\begin{pmatrix} \varepsilon_{\alpha_1} \\ \varepsilon_{\beta_1} \\ \varepsilon_{\alpha_1\beta_1} \end{pmatrix} = [T]^{-1} \begin{bmatrix} C_{11} & C_{12} & C_{13} \\ C_{21} & C_{22} & C_{23} \\ C_{31} & C_{32} & C_{33} \end{bmatrix} [T] \begin{pmatrix} \sigma_{\alpha_1} \\ \sigma_{\beta_1} \\ \tau_{\alpha_1\beta_1} \end{pmatrix} \tag{50}$$

The coordination transformation matrix $[T]$ is given as,

$$\Big[T\Big] = \begin{bmatrix} cos^2\theta^1 & sin^2\theta^1 & 2sin\theta^1 cos\theta^1 \\ sin^2\theta^1 & cos^2\theta^1 & -2sin\theta^1 cos\theta^1 \\ -sin\theta^1 cos\theta^1 & sin\theta^1 cos\theta^1 & cos^2\theta^1 - sin^2\theta^1 \end{bmatrix} \tag{51}$$

Here, stress and strain relationship in (α_1, β_1) coordinate system can also be expressed in the following form,

$$\begin{pmatrix} \varepsilon_{\alpha_1} \\ \varepsilon_{\beta_1} \\ \varepsilon_{\alpha_1\beta_1} \end{pmatrix} = \begin{bmatrix} C'_{11} & C'_{12} & C'_{13} \\ C'_{21} & C'_{22} & C'_{23} \\ C'_{31} & C'_{32} & C'_{33} \end{bmatrix} \begin{pmatrix} \sigma_{\alpha_1} \\ \sigma_{\beta_1} \\ \tau_{\alpha_1\beta_1} \end{pmatrix} \tag{52}$$

Then the Eq. 51 and 52 lead to following equation,

$$\begin{bmatrix} C'_{11} & C'_{12} & C'_{13} \\ C'_{21} & C'_{22} & C'_{23} \\ C'_{31} & C'_{32} & C'_{33} \end{bmatrix} = [T]^{-1} \begin{bmatrix} C_{11} & C_{12} & C_{13} \\ C_{21} & C_{22} & C_{23} \\ C_{31} & C_{32} & C_{33} \end{bmatrix} [T]. \tag{53}$$

Note in the above equation that C'_{i2} (for $i = 1, 2, 3$) terms are known based on the analysis presented in the preceding section. However, the C_{ij} terms (constitutive matrix as per the x, y coordinate system) are not known and we need to obtain these terms. Based on the above equation, we have

$$\begin{aligned} C'_{12} &= C_{12}cos^4\theta^1 - (-C_{13} + 2C_{32})cos^3\theta^1 sin^3\theta^1 + (C_{11} + C_{22} - 2C_{33})cos^2\theta^1 sin^2\theta^1 \\ &+ (C_{23} - C_{31})cos^2\theta^1 sin^3\theta^1 + C_{21}sin^4\theta^1, \\ C'_{22} &= C_{22}cos^4\theta^1 + (C_{23} + 2C_{32})cos^3\theta^1 sin\theta^1 + (C_{12} + C_{21} + 2C_{33})cos^2\theta^1 sin^2\theta^1 \\ &+ (C_{13} + 2C_{31})cos\theta^1 sin^3\theta^1 + C_{11}sin^4\theta^1, \\ C'_{32} &= C_{32}cos^4\theta^1 + (C_{12} - C_{22} + C_{33})cos^3\theta^1 sin\theta^1 + (-C_{23} + C_{31} - C_{32} + C_{13})cos^2\theta^1 sin^2\theta^1 \\ &+ (C_{11} - C_{21} - C_{33})cos\theta^1 sin^3\theta^1 - C_{31}sin^4\theta^1. \end{aligned} \tag{54}$$

In similar way, by transforming the (x, y) coordinate system to the (α_2, β_2) coordinate system, we have

$$\begin{aligned}
C''_{12} &= C_{12}cos^4\theta^2 - (-C_{13} + 2C_{32})cos^3\theta^2 sin^3\theta^2 + (C_{11} + C_{22} - 2C_{33})cos^2\theta^2 sin^2\theta^2 \\
&+ (C_{23} - C_{31})cos^2\theta^2 sin^3\theta^2 + C_{21}sin^4\theta^2, \\
C''_{22} &= C_{22}cos^4\theta^2 + (C_{23} + 2C_{32})cos^3\theta^2 sin\theta^2 + (C_{12} + C_{21} + 2C_{33})cos^2\theta^2 sin^2\theta^2 \\
&+ (C_{13} + 2C_{31})cos\theta^2 sin^3\theta^2 + C_{11}sin^4\theta^2, \\
C''_{32} &= C_{32}cos^4\theta^2 + (C_{12} - C_{22} + C_{33})cos^3\theta^2 sin\theta^2 + (-C_{23} + C_{31} - C_{32} + C_{13})cos^2\theta^2 sin^2\theta^2 \\
&+ (C_{11} - C_{21} - C_{33})cos\theta^2 sin^3\theta^2 - C_{31}sin^4\theta^2
\end{aligned} \tag{55}$$

Further, following a similar approach between the (x, y) coordinate system to the (α_3, β_3) coordinate system, we have

$$\begin{aligned}
C'''_{12} &= C_{12}cos^4\theta^3 - (-C_{13} + 2C_{32})cos^3\theta^3 sin^3\theta^3 + (C_{11} + C_{22} - 2C_{33})cos^2\theta^3 sin^2\theta^3 \\
&+ (C_{23} - C_{31})cos^2\theta^3 sin^3\theta^3 + C_{21}sin^4\theta^3, \\
C'''_{22} &= C_{22}cos^4\theta^3 + (C_{23} + 2C_{32})cos^3\theta^3 sin\theta^3 + (C_{12} + C_{21} + 2C_{33})cos^2\theta^3 sin^2\theta^3 \\
&+ (C_{13} + 2C_{31})cos\theta^3 sin^3\theta^3 + C_{11}sin^4\theta^3, \\
C'''_{32} &= C_{32}cos^4\theta^3 + (C_{12} - C_{22} + C_{33})cos^3\theta^3 sin\theta^3 + (-C_{23} + C_{31} - C_{32} + C_{13})cos^2\theta^3 sin^2\theta^3 \\
&+ (C_{11} - C_{21} - C_{33})cos\theta^3 sin^3\theta^3 - C_{31}sin^4\theta^3
\end{aligned} \tag{56}$$

The value of local elastic moduli of element 1 (C'_{12}, C'_{22}, and C'_{32}), local elastic moduli of element 2 (C''_{12}, C''_{22}, and C''_{32}) and local elastic moduli of element 3 (C'''_{12}, C'''_{22}, and C'''_{32}) are already known from previous sections. Therefore, nine components of C_{ij} (refer to Eq. 4) can be determined by solving these nine simultaneous equations given in Eqs. 54, 55 and 56.

In this context, it may be noted that the effective in-plane Young's moduli, shear modulus and Poisson's ratios can be obtained directly from the in-plane constitutive matrix presented in Eq. 4. The relation between elastic moduli and in-plane constitutive matrix elements is provided below in Eq. 57.

$$E_1 = \frac{1}{C_{11}} \qquad E_2 = \frac{1}{C_{22}} \qquad G_{12} = \frac{1}{C_{33}} \qquad \nu_{12} = -C_{12} \times E_2 \qquad \nu_{21} = -C_{21} \times E_1 \tag{57}$$

In the following section, we present numerical results to explore the bi-level expanded design space of the proposed asymmetric lattices.

3. Results and discussion

A detailed numerical study is performed here to assess the effect of different design parameters covering the bi-level space of architected lattices on the effective elastic properties of regular (non-auxetic) and auxetic honeycombs. The unit cell level architecture includes the cell angles, and lengths of different

cell walls, while the beam level architecture includes variably-thickened cell wall parameters ζ_i and η_i ($i = 1, 2, 3$) along with the multi-material ratio parameter (q, where $E_1 = E_2 = qE_3 = E_s$, refer to Figs. 1(f)) and 3(b). We have first presented extensive validations of the proposed analytical framework considering various cases of hexagonal honeycomb lattices available in the literature, (1) asymmetric monomaterial honeycombs without beam-level architecture considering beam-level bending, shear and axial deformations, (2) symmetric monomaterial honeycombs without beam-level architecture considering beam-level bending, shear and axial deformations (separate cases of non-auxetic and auxetic architectures), (3) symmetric monomaterial honeycombs without beam-level architecture considering only beam-level bending deformations (separate cases of non-auxetic and auxetic architectures), (4) multi-material symmetric lattices with auxetic and non-auxetic configurations considering only beam-level bending deformation, (5) multi-material symmetric lattices with auxetic and non-auxetic configurations considering beam-level bending, shear and axial deformations. Note that all these cases can be readily evaluated based on the generic analytical formulation presented in the preceding section. Such multi-stage validations considering the crucial factors of the proposed lattice (such as asymmetry, multi-material architecture, unit cell level auxetic and non-auxetic geometries, and beam-level deformation mechanics) would provide necessary confidence in the developed analytical framework. Subsequently, new results are presented concerning the bi-level architected multi-material design space.

3.1. Validation of the proposed analytical framework

The proposed analytical framework can obtain the entire elastic constitutive matrix of a generic lattice having multi-material asymmetric unit cell with variably-thickened beam-level architecture. The effective elastic moduli, like in-plane Young's moduli, shear modulus and Poisson's ratios can also be readily obtained from the constitutive matrix. Plenty of special lattice classes can be obtained directly based on the analytical framework (as shown in Fig. 1, in addition to different beam-level architecture and multi-material configurations). Further, different levels of accuracy and computational efficiency can be ascertained by adopting the beam-level deformation mechanics accordingly involving bending, axial and shear deformations. It can be noted here that the effect of shear and axial deformation becomes crucial as the cell walls get thicker and axially more flexible, respectively.

First, the proposed analytical framework is validated with the results of Chen and Yang [46] which are available for asymmetric mono-material honeycombs ($t_1 = t_2 = t_3 = 1mm$, $\eta_1 = \eta_2 = \eta_3 = 1$, and $\zeta_1 = \zeta_2 = \zeta_3 = 1$), as shown in Table 1. The results (obtained from the present formulation and available literature) are compared for two models, such as Model A ($L_1 = L_2 = L_3 = L = 10mm$, $\theta_2 = 40°$, $\theta_3 = 80°$) and Model B ($L_1 = 24.5mm, L_2 = 6mm, L_3 = 10mm$; $\theta_2 = 26.3°$, $\theta_3 = 88.7°$) under different

Table 1: Validation for asymmetric mono-material hexagonal lattices based on comparing results obtained from the current analytical approach, results from literature and finite element method. Here we compare the present results with analytical and the finite element (FE) results from literature [46] considering asymmetric mono-material ($E_1 = E_2 = E_3 = E_s$) hexagonal cells. The non-dimensionalized elastic parameters for non-auxetic asymmetric honeycombs ($t_1 = t_2 = t_3 = t$, $\eta_1 = \eta_2 = \eta_3 = 1$, and $\zeta_1 = \zeta_2 = \zeta_3 = 1$) are compared for different wall thickness under the consideration of bending, axial and shear deformation of cell walls. In model A, the length of the three cell walls is same ($L_1 = L_2 = L_3 = L = 10mm$), but the angles between the walls are different ($\theta_2 = 40°, \theta_3 = 80°$). In model B, the lengths and angles of the cell walls are different ($L_1 = 24.5mm, L_2 = 6mm, L_3 = 10mm$; $\theta_2 = 26.3°, \theta_3 = 88.7°$). However, in both models A and B, the thickness of the cell walls is the same, $t_1 = t_2 = t_3 = t$. The results are compared for three thicknesses t =0.1, 0.5, 1mm under three cases: (a), b and (c). In Case (a) only the bending effect is considered in the analysis (B). In Case (b) only bending and axial effects are considered in the analysis (Be.+Ax.). In Case (c) all bending, axial and shear effects are considered in the analysis (Be.+Ax.+Sh.).

Model A		**Case (a), (Be.)**		**Case (b), (Be.+Ax.)**		**Case (c), (Be.+Ax.+Sh.)**		**FEM [46]**
	t	**Present**	**Chen [46]**	**Present**	**Chen [46]**	**Present**	**Chen [46]**	
$\frac{1}{(C_{12}E_s)}$	0.1	-3.267×10^{-6}	-3.267×10^{-6}	-3.267×10^{-6}	-3.267×10^{-6}	-3.267×10^{-6}	-3.267×10^{-6}	-3.267×10^{-6}
	0.5	-4.084×10^{-4}	-3.267×10^{-6}	-4.094×10^{-4}	-4.094×10^{-4}	-4.068×10^{-4}	-4.068×10^{-4}	-4.068×10^{-4}
	1	-3.267×10^{-3}	-3.267×10^{-3}	-3.300×10^{-3}	-3.300×10^{-3}	-3.216×10^{-3}	-3.216×10^{-3}	-3.216×10^{-3}
$\frac{1}{(C_{22}E_s)}$	0.1	3.111×10^{-6}	3.111×10^{-6}	3.110×10^{-6}	3.110×10^{-6}	3.109×10^{-6}	3.109×10^{-6}	3.109×10^{-6}
	0.5	3.889×10^{-4}	3.889×10^{-4}	3.851×10^{-4}	3.851×10^{-4}	3.826×10^{-4}	3.826×10^{-4}	3.826×10^{-4}
	1	3.111×10^{-3}	3.111×10^{-3}	2.991×10^{-3}	2.991×10^{-3}	2.918×10^{-3}	2.918×10^{-3}	2.918×10^{-3}
$\frac{1}{(C_{32}E_s)}$	0.1	4.841×10^{-6}	4.841×10^{-6}	4.841×10^{-6}	4.841×10^{-6}	4.839×10^{-6}	4.839×10^{-6}	4.839×10^{-6}
	0.5	6.051×10^{-4}	6.051×10^{-4}	6.052×10^{-4}	6.052×10^{-4}	6.013×10^{-4}	6.013×10^{-4}	6.013×10^{-4}
	1	4.841×10^{-3}	$.841\times10^{-3}$	4.845×10^{-3}	4.845×10^{-3}	4.722×10^{-3}	4.722×10^{-3}	4.722×10^{-3}

Model B		**Case (a), (Be.)**		**Case (b), (Be.+Ax.)**		**Case (c), (Be.+Ax.+Sh.)**		**FEM [46]**
	t	**Present**	**Chen [46]**	**Present**	**Chen [46]**	**Present**	**Chen [46]**	
$\frac{1}{(C_{12}E_s)}$	0.1	-1.584×10^{-5}	-1.58×10^{-5}	-1.584×10^{-5}	-1.584×10^{-5}	-1.583×10^{-5}	-1.583×10^{-5}	-1.583×10^{-5}
	0.5	-1.980×10^{-3}	-1.98×10^{-3}	-1.993×10^{-3}	-1.993×10^{-3}	-1.959×10^{-3}	-1.959×10^{-3}	-1.959×10^{-3}
	1	-1.584×10^{-2}	-1.584×10^{-2}	-1.627×10^{-2}	-1.627×10^{-2}	-1.520×10^{-2}	-1.520×10^{-2}	-1.520×10^{-2}
$\frac{1}{(C_{22}E_s)}$	0.1	3.225×10^{-5}	3.225×10^{-5}	3.212×10^{-5}	3.212×10^{-5}	3.211×10^{-5}	3.212×10^{-5}	3.212×10^{-5}
	0.5	4.031×10^{-3}	4.031×10^{-3}	3.673×10^{-3}	3.673×10^{-3}	3.637×10^{-3}	3.637×10^{-3}	3.637×10^{-3}
	1	3.225×10^{-2}	3.225×10^{-2}	2.320×10^{-2}	2.320×10^{-2}	2.250×10^{-2}	2.250×10^{-2}	2.250×10^{-2}
$\frac{1}{(C_{32}E_s)}$	0.1	9.427×10^{-6}	9.427×10^{-6}	9.426×10^{-6}	9.426×10^{-6}	9.424×10^{-6}	9.424×10^{-6}	9.424×10^{-6}
	0.5	1.178×10^{-3}	1.178×10^{-3}	1.178×10^{-3}	1.178×10^{-3}	1.170×10^{-3}	1.170×10^{-3}	1.170×10^{-3}
	1	9.427×10^{-3}	9.427×10^{-3}	9.406×10^{-3}	9.406×10^{-3}	9.178×10^{-3}	9.178×10^{-3}	9.178×10^{-3}

wall thicknesses t =0.1, 0.5, 1mm. The non-dimensionalized elastic constitutive constants ($1/(C_{12}\ E_s)$, $1/(C_{22}\ E_s)$ and $1/(C_{32}\ E_s)$ are compared for three cases (a), (b) and (c). In Case (a) only bending effect is considered in the analysis (Be.), and in Case (b), only bending and axial effects are considered in the analysis (Be.+Ax.). Whereas in Case (c), all bending, axial and shear effects are considered in the analysis (Be.+Ax.+Sh.). The corresponding finite element results [46] are also tabulated in Table 1. The comparison presented in Table 1 shows excellent agreement for all the cases, establishing that the

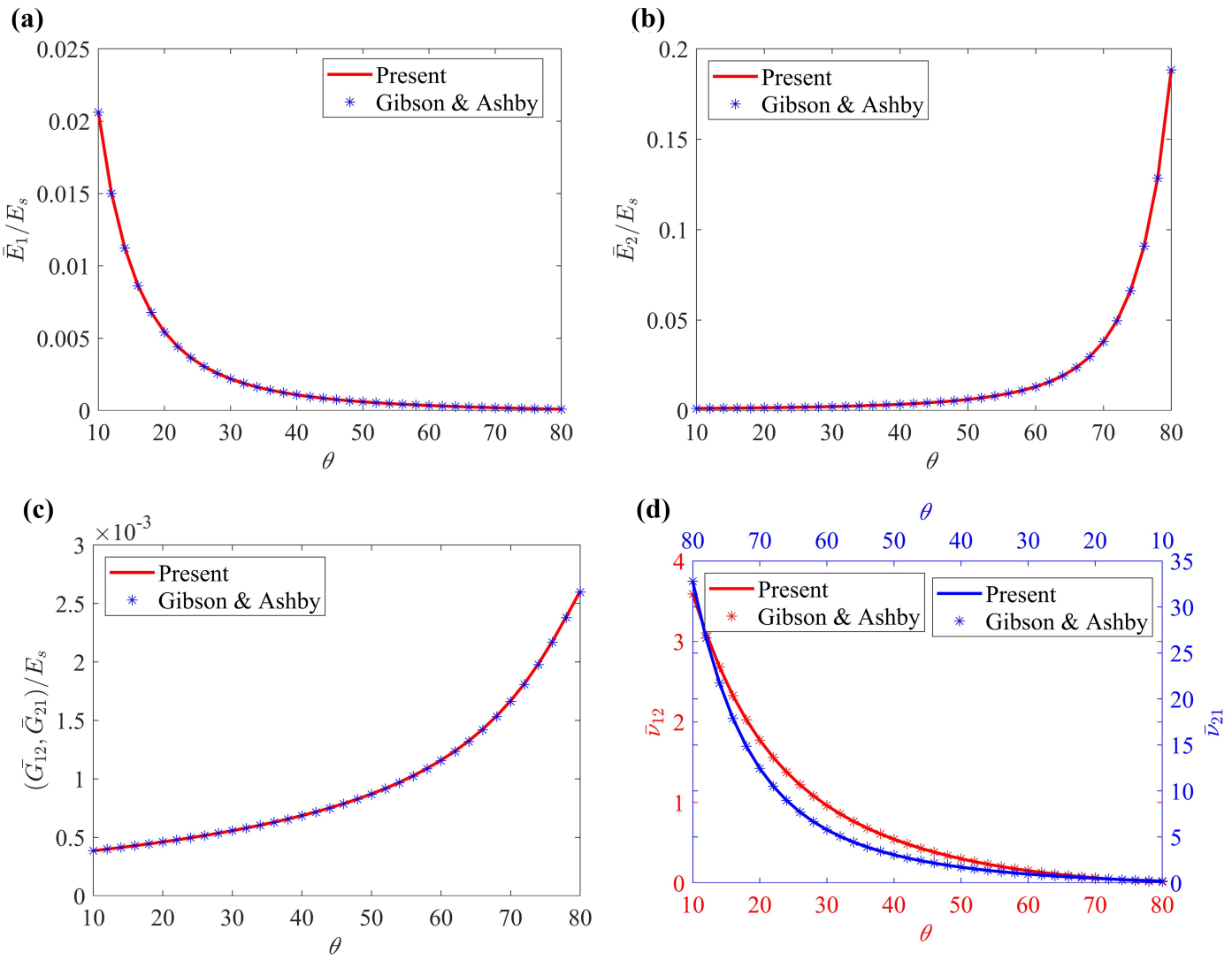

Figure 4: Validation for regular (non-auxetic) symmetric mono-material honeycombs under axial, bending and shear effects. Comparison of present results with the classical approach of Gibson and Ashby [37] in which the closed-form expression of effective Young's moduli, shear moduli and Poisson's ratios for perfectly periodic regular mono-material ($E_1 = E_2 = E_3 = E_s$) hexagonal cells are derived for both directions by applying stress in each direction individually. The non-dimensionalized value of the elastic parameter for non-auxetic (regular) honeycombs ($L_1 = L_2 = L_3 = L = 1mm$, $t_1 = t_2 = t_3 = 0.1L$, $\eta_1 = \eta_2 = \eta_3 = 1$, and $\zeta_1 = \zeta_2 = \zeta_3 = 1$) are compared considering different cell angles under the consideration of axial, bending and shear deformations of cell walls. Variations with respect to cell angle θ (in degree) are presented for **(a, b)** Young's moduli $\bar{E}_1$ and $\bar{E}_2$ **(c)** shear moduli $\bar{G}_{12}$ or $\bar{G}_{21}$ **(d)** Poisson's ratios $\bar{\nu}_{12}$ or $\bar{\nu}_{21}$. The normalization of the elastic moduli is carried out with respect to intrinsic Young's modulus (E_s) of walls. It should be noted that the Poisson's ratios ($\bar{\nu}_{12}$ and $\bar{\nu}_{21}$) do not depend on the intrinsic material properties of the wall members.

effect of asymmetry can be accurately analyzed through the present analytical approach.

Further, the present analytical approach is validated with the closed-form expressions of Gibson and Ashby [37] available for symmetric mono-material hexagonal honeycombs ($L_1 = L_2 = L_3 = L = 1mm$, $t_1 = t_2 = t_3 = 0.1L$, $\eta_1 = \eta_2 = \eta_3 = 1$, and $\zeta_1 = \zeta_2 = \zeta_3 = 1$), as shown in Figs. SM1.S1, 4, SM1.S2 and SM1.S3 considering non-auxetic and auxetic configurations along with different beam-level deformation mechanics (bending, axial and shear deformations). In Fig. SM1.S1, the variation of non-dimensionalized Young's moduli ($\bar{E}_1/E_s$, $\bar{E}_2/E_s$), shear moduli ($\bar{G}_{12}/E_s$ and $\bar{G}_{21}/E_s$) and Poisson's ratios ($\bar{\nu}_{12}$ and

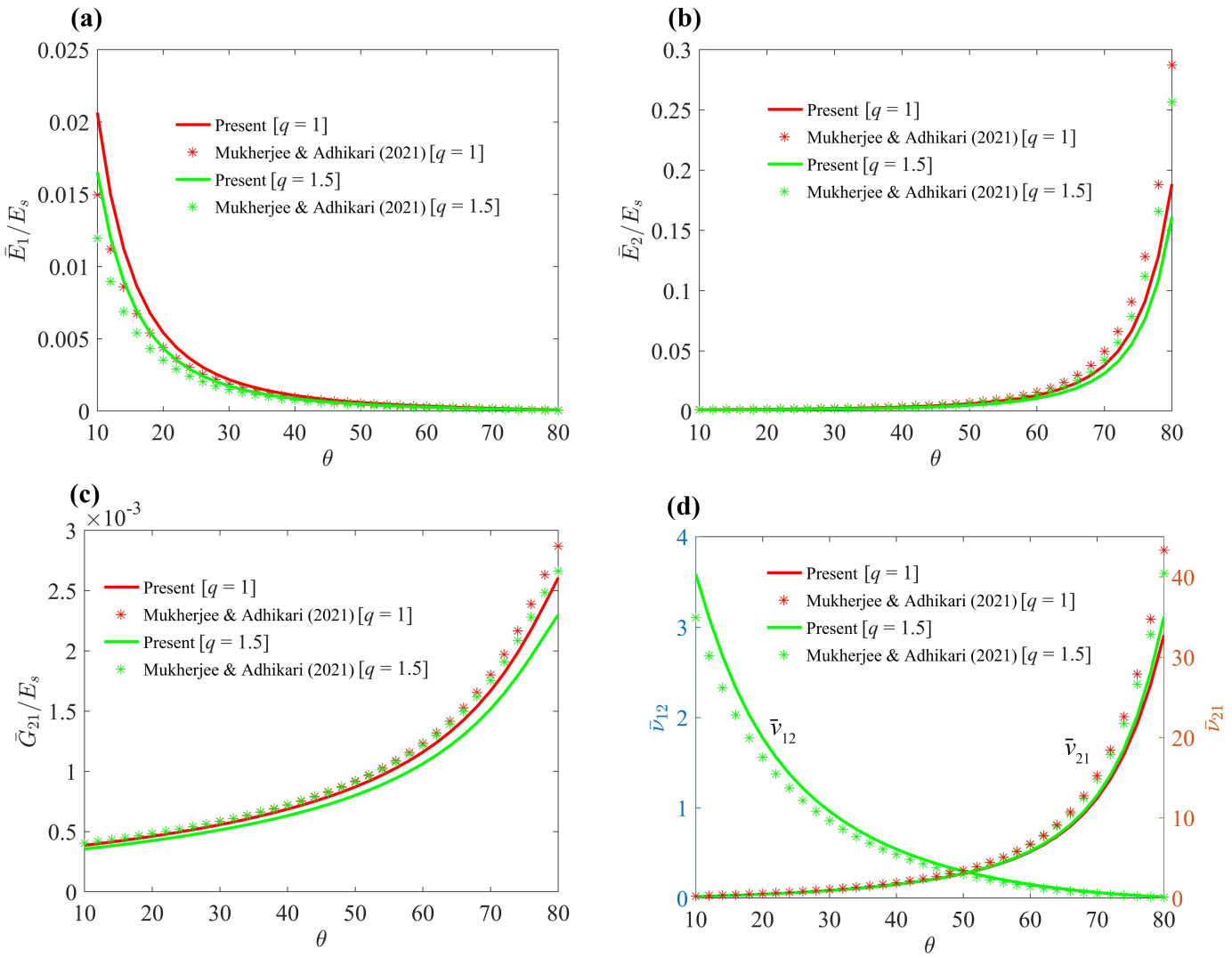

Figure 5: Validation with Timoshenko theory-based beam model for multi-material (non-auxetic) symmetric honeycombs (considering beam-level bending, shear and axial deformation). Comparison of present results with Timoshenko theory based beam model of Mukherjee and Adhikari [68]. The non-dimensionalized value of elastic moduli for non-auxetic multi-material honeycombs ($E_1 = E_2 = qE_3 = E_s$, $L_1 = L_2 = L_3 = L = 1mm$, $t_1 = t_2 = t_3 = 0.1L$, $\eta_1 = \eta_2 = \eta_3 = 1$, and $\zeta_1 = \zeta_2 = \zeta_3 = 1$) are compared for different cell angles under the consideration of axial, shear and bending deformations of cell walls. Variations with respect to cell angle θ (in degree) considering two different material ratios, q are presented for **(a, b)** Young's moduli $\bar{E}_1$ and $\bar{E}_2$ **(c)** shear moduli $\bar{G}_{12}$ or $\bar{G}_{21}$ **(d)** Poisson's ratios $\bar{\nu}_{12}$ and $\bar{\nu}_{21}$. The normalization of Young's moduli ($\bar{E}_1$, $\bar{E}_2$) and shear moduli ($\bar{G}_{12}$, $\bar{G}_{21}$) is carried out with respect to intrinsic Young's modulus (E_s). It should be noted that the Poisson's ratios are non-dimensional quantities.

$\bar{\nu}_{21}$) are compared for regular (non-auxetic) honeycombs by considering the bending effect only for a wide range of cell wall angles θ (10° to 80°). Here ($\bar{\bullet}$) represents an effective elastic modulus of the lattice that is non-dimensionalized with respect to the intrinsic material property E_s of a mono-material configuration. Note that the Poisson's ratios are already non-dimensional. Similarly, the variation of non-dimensionalized Young's moduli, shear moduli and Poisson's ratios are compared for regular (non-auxetic) honeycombs in Fig. 4 considering the effect axial, shear and bending deformations of the cell walls. Further, the non-dimensionalized elastic properties for auxetic honeycombs are compared in

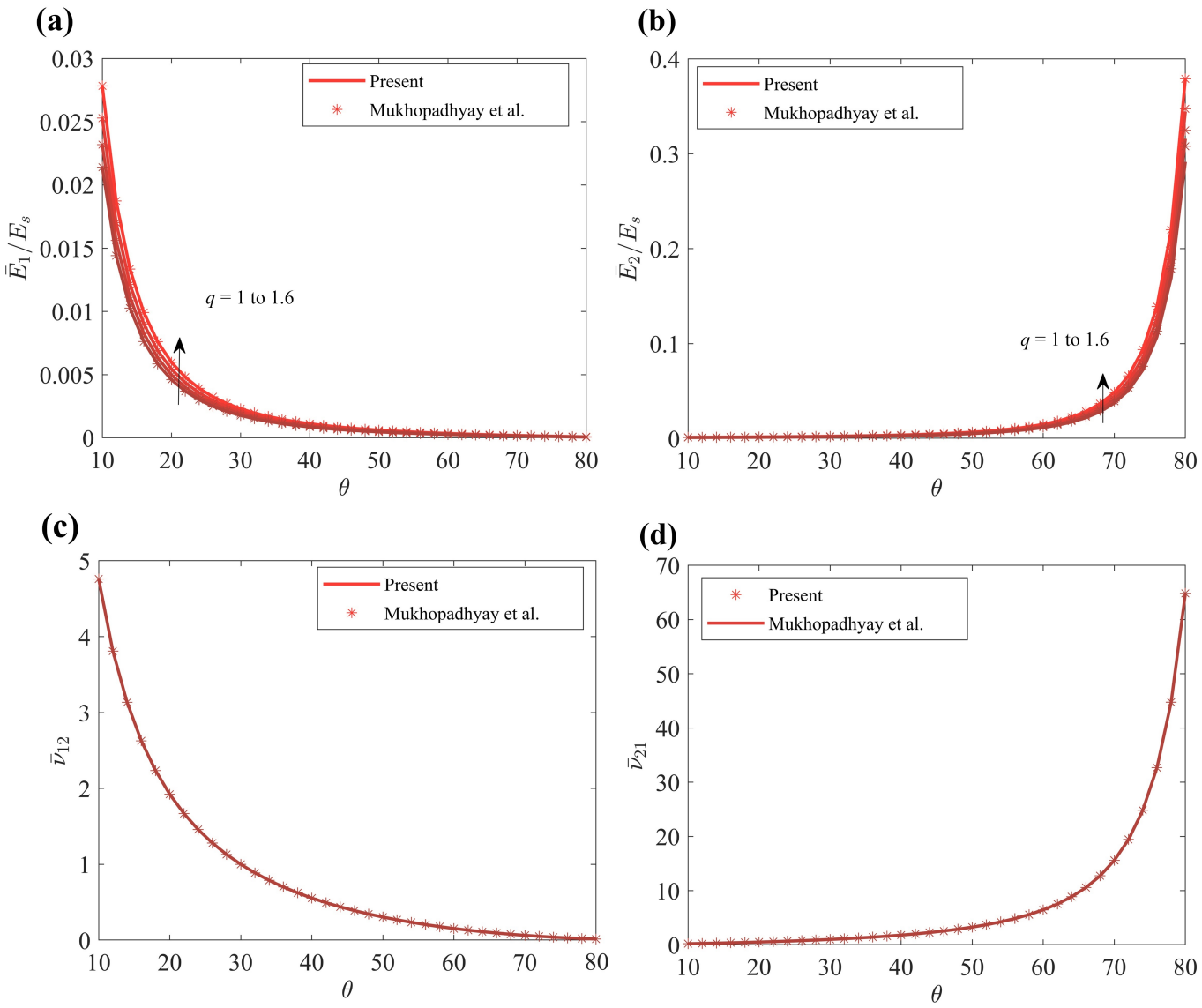

Figure 6: Validation for non-auxetic symmetric multi-material honeycombs only under beam-level bending deformation. Comparison of present results with the classical approach of Mukhopadhyay et al. [60] in which the closed-form expression of Young's moduli and Poisson's ratios for multi-material ($E_1 = E_2 = qE_3 = E_s$) hexagonal cells are derived under bending deformation for both directions by applying stress in each direction individually. The non-dimensionalized values of the elastic parameters for regular (non-auxetic) honeycombs ($L_1 = L_2 = L_3 = L = 1mm$, $t_1 = t_2 = t_3 = 0.1L$, $\eta_1 = \eta_2 = \eta_3 = 1$, and $\zeta_1 = \zeta_2 = \zeta_3 = 1$) are compared for different cell angles under only bending deformation of cell walls. The variation of equivalent elastic parameters is plotted for different multi-material ratios (q =1 to 1.6). Variations with respect to cell angle θ (in degree) considering different material ratios (q) are presented for **(a, b)** Young's moduli $\bar{E}_1$ and $\bar{E}_2$, and **(c, d)** Poisson's ratios $\bar{\nu}_{12}$ and $\bar{\nu}_{21}$. The normalization of the Young's moduli ($\bar{E}_1$, $\bar{E}_2$) is carried out with respect to intrinsic Young's modulus (E_s) of the wall with length L. In these figures, the arrows depict the increasing trend of multi-material ratio (q) from lower value ($q = 1$, which represents mono-material) to large value ($q = 1.6$, which represents multi-material with higher ratio). The Poisson's ratios $\bar{\nu}_{12}$, $\bar{\nu}_{21}$ show independence from the multi-material ratio (q) as it does not depend on the intrinsic material properties of the cell wall members. These quantities only depend on the structural geometry of the lattice.

Figs. SM1.S2 and SM1.S3. In Fig. SM1.S2, results are compared only by condensing the bending effect of cell walls for both cases. In Fig. SM1.S3, results are compared for the case in which the effect of axial, shear, and bending deformation of cell walls is taken into consideration. Excellent agreement is observed for both regular (non-auxetic) and auxetic honeycombs under the consideration of different

beam-level deformation mechanics. It is also worth noting here that the Poisson's ratios ($\bar{\nu}_{12}$ and $\bar{\nu}_{21}$) do not depend on the intrinsic material properties of the cell wall members.

The concept of multi-material hexagonal honeycombs (symmetric structure) and concerned analyses of effective elastic moduli were first presented by Mukhopadhyay et al. [60]. In that analysis, beam-level deformation was considered based on bending with the assumption of thin cell walls. Subsequently, the same approach was extended for thick cell walls through the incorporation of beam-level shear and axial deformation effects by Mukherjee and Adhikari [68]. Here, the present framework is validated with Euler-Bernoulli and Timoshenko beam theory-based approach presented by Mukhopadhyay et al. [60] and Mukherjee and Adhikari [68] in Figs. 5, 6, and SM1.S4 to SM1.S7. The non-dimensionalized equivalent elastic properties ($\bar{E}_1/E_s$, $\bar{E}_2/E_s$, $\bar{G}_{12}/E_s$, and $\bar{\nu}_{12}/\ \bar{\nu}_{21}$) are compared under different cell wall angle θ (10° to 80°) considering mono-material and multi-material configurations (auxetic and non-auxetic). Excellent agreement is observed between both the approaches considering different beam-level deformation mechanisms (a. only bending, b. bending and axial, c. bending, axial and shear). In this context, it may be noted that the effective elastic moduli of the hexagonal lattices can be tuned by introducing the proper multi-material ratio, whereas the Poisson's ratios $\bar{\nu}_{12},\ \bar{\nu}_{21}$ show independence (primarily in the predominant beam-level transverse deformation mechanism) from the multi-material ratio (q) as it does not depend on the intrinsic material properties of the cell wall members. The Poisson's ratios of hexagonal lattices mostly depend on the unit cell level geometry.

Having adequate confidence in the developed analytical framework based on extensive multi-stage validations with existing literature, we embark on further numerical explorations in the following section concerning the proposed bi-level architected multi-material asymmetric lattices.

3.2. Numerical investigation on the constitutive behavior

After validating the present approach, it is further utilized to obtain the complete in-plane constitutive, (C_{ij}) matrix of various thick and thin-walled multi-material honeycomb lattices. In this section, we investigate the effect of different influencing factors systematically, as explained below:

(1) Effect of the multimaterial parameter, considering non-auxetic and auxetic symmetric configurations along with different beam-level deformation mechanics are shown in Fig. 7, and SM1.S8 to SM1.S10. Similar sets of results for two other wall thickness values (relatively thinner and thicker, respectively) are shown in Fig. SM2.S1 to SM2.S8.

(2) Combined effect of asymmetry and the multimaterial parameter, considering non-auxetic and auxetic configurations including coupled beam-level bending, axial and shear deformations are shown in

Fig. 8 and SM1.S11. Similar sets of results for two other wall thickness values (relatively thinner and thicker, respectively) are shown in Fig. SM2.S9 to SM2.S12.

(3) Effect of the beam-level architecture in terms of the thickened length ratio ζ_i, considering non-auxetic and auxetic symmetric configurations along with different beam-level deformation mechanics are shown in Fig. 9, and SM1.S12 to SM1.S14. Similar sets of results for two other wall thickness values (relatively thinner and thicker, respectively) are shown in Fig. SM2.S13 to SM2.S20.

(4) Combined effect of asymmetry and beam-level architecture in terms of the thickened length ratio ζ_i, considering non-auxetic and auxetic configurations including coupled beam-level bending, axial and shear deformations are shown in Fig. 10 and SM1.S15. Similar sets of results for two other wall thickness values (relatively thinner and thicker, respectively) are shown in Fig. SM2.S21 to SM2.S24.

(5) Effect of the beam-level architecture in terms of the thickness ratio η_i, considering non-auxetic and auxetic symmetric configurations along with different beam-level deformation mechanics are shown in Fig. 11, and SM1.S16 to SM1.S18. Similar sets of results for two other wall thickness values (relatively thinner and thicker, respectively) are shown in Fig. SM2.S25 to SM2.S32.

(6) Combined effect of asymmetry and beam-level architecture in terms of the thickness ratio η_i, considering non-auxetic and auxetic configurations including coupled beam-level bending, axial and shear deformations are shown in Fig. 12 and SM1.S19. Similar sets of results for two other wall thickness values (relatively thinner and thicker, respectively) are shown in Fig. SM2.S33 to SM2.S36.

(7) Effect of cell wall thickness, considering non-auxetic and auxetic symmetric configurations along with different beam-level deformation mechanics are shown in Fig. 13, and SM1.S20 to SM1.S22.

(8) Combined effect of asymmetry and cell wall thickness, considering non-auxetic and auxetic configurations including coupled beam-level bending, axial and shear deformations are shown in Fig. 14 and SM1.S23.

(9) Effect of cell wall length ratio, considering non-auxetic and auxetic symmetric configurations along with different beam-level deformation mechanics are shown in Fig. 15, and SM1.S24 to SM1.S26. Similar sets of results for two other wall thickness values (relatively thinner and thicker, respectively) are shown in Fig. SM2.S37 to SM2.S44.

(10) Combined effect of asymmetry and cell wall length ratio, considering non-auxetic and auxetic configurations including coupled beam-level bending, axial and shear deformations are shown in Fig. 16 and SM1.S27. Similar sets of results for two other wall thickness values (relatively thinner and thicker, respectively) are shown in Fig. SM2.S45 to SM2.S48.

(11) *Supplementary material:* The results mentioned in points (1) to (10) above for the main manuscript

and supplementary material 1 (SM1) are obtained for $t/L = 0.2$, unless otherwise mentioned. For a comprehensive understanding, we provide additional numerical results in supplementary material 2 (SM2) for the above cases considering two other cell wall thicknesses, as $t/L = 0.1$ (thinner) and 0.3 (thicker).

In Fig. SM1.S8 and 7, the variation of all in-plane constitutive constants for non-auxetic multi-material honeycombs ($E_1 = E_2 = qE_3 = E_s$, $L_1 = L_2 = L_3 = L = 1$mm, $t_1 = t_2 = t_3 = 0.2L$, $\eta_1 = \eta_2 = \eta_3 = 1$, and $\zeta_1 = \zeta_2 = \zeta_3 = 1$) is plotted considering different cell angles ($\theta = 10^\circ$ to 80°). Similar variations of in-plane constitutive constants for other thicknesses $t_1 = t_2 = t_3 = 0.1L, 0.3L$ are shown in Fig. SM2.S1, SM2.S2, SM2.S3 and SM2.S4 of the supplementary material. The behavior of each in-plane constitutive constant is plotted for different multi-material ratios (q =1 to 2) and cell angle θ. The normalization of the constitutive constants (C_{ij}) is carried out with respect to intrinsic Young's modulus (E_s) of the vertical wall with length L. In these figures, the arrows depict the increasing values of multi-material ratio (q) from lower value ($q = 1$, which represents mono-material) to large value ($q = 2$, which represents multi-material with higher ratio). In Figs. SM1.S8, SM2.S1 and SM2.S2, the variation of all in-plane constitutive constants are presented by considering only bending deformations of cell walls in the analysis. Similarly, corresponding variations of in-plane constitutive constants are presented in the Figs. 7, SM2.S3 and SM2.S4 under the consideration of axial, bending and shear deformations of cell walls. In general, it is observed that all in-plane constitutive constants of honeycomb structures are affected significantly by multi-material ratio (q) for different cell angles θ. The results demonstrate that the elastic properties of a honeycomb can be effectively modulated by introducing multi-material unit cells ($q = E_1/E_3 = E_2/E_3$) without altering the unit cell shapes. The effect of multi-material ratio is more influential for C_{12} / C_{21}, C_{13} / C_{31} and C_{23} / C_{32}, whereas it's effect on the other elastic constitutive constants like C_{11}, C_{22} and C_{33} is comparatively less. The values of C_{12} and C_{21} decrease by 1.5 times as the value of q is increased from 1 to 2, whereas the value of C_{13} / C_{31} decreases and C_{23} / C_{32} increases by 3 to 6 times as q is increased from 1 to 2. The corresponding effect of multi-material ratio (q) on C_{11}, C_{22} and C_{33} are comparatively less and their values increase by 50% to 100% for different cell angle θ as q is increased from 1 to 2. The results show that the effect of multi-material ratio depends upon the cell angle θ, the trends of which change depending on the constitutive constant under consideration. From the comparison of Figs. SM1.S8, SM2.S3 and SM2.S4 with Figs. 7, SM2.S1 and SM2.S2, it is also observed that each elastic constitutive constants have significant contribution of axial and shear effect of cell walls. The magnitude of each in-plane constitutive constant increases by 10-20% for thinner-walled ($t/L = 0.1$), 20-30% for moderately thick-walled (($t/L = 0.2$) and 30-40% thicker-walled honeycombs (($t/L = 0.3$), when the effects of axial and shear deformations of cell walls

are considered along with the bending deformation. However, the trend of variation of all constitutive constants with respect to cell wall angle (θ) remains unchanged under axial, shear and bending effects consideration as compared to the only bending case.

The variation of all in-plane constitutive constants for auxetic multi-material honeycombs is plotted for different cell angles in Fig. SM1.S9 and SM1.S10 considering a range of multi-material ratios (q =1 to 2) and $t/L = 0.2$. Further, similar results for auxetic honeycombs are presented for two other cell wall thicknesses ($t/L = 0.1, 0.3$) in supplementary material, Figs. SM2.S5 to SM2.S8. In the Figs. SM1.S9, SM2.S5 and SM2.S6, variations of all in-plane constitutive constants are presented by considering only the bending deformation effect of cell walls. Similarly, corresponding variations of constitutive constants under axial, bending and shear deformation effects of cell walls are shown in Figs. SM1.S10, SM2.S7 and SM2.S8. It is noted that all the in-plane constitutive constants get affected significantly for auxetic configurations with the variation of cell angle θ and the multimaterial parameter q. For C_{11}, C_{12} and C_{21}, the maximum effect of multi-material ratio is observed at cell wall angle 45°, whereas the effect is most notable in C_{13}, C_{31}, C_{23} and C_{32} for the cell wall angles more than 60°. Maximum change for C_{22} is noted for the cell wall angles lower than 40°. The trends of variations are similar under the consideration of only bending deformation, and the combined effect of bending, axial and shear deformations. However, the magnitude of each constitutive constant increases by 10-20% for thinner-walled ($t/L = 0.1$), 20-30% for moderately thick-walled (($t/L = 0.2$) and 30-40% for thicker-walled honeycombs ($t/L = 0.3$) with the consideration of axial and shear effect of cell walls along with the bending deformation.

In addition to the regular symmetric case, the asymmetric multi-material lattices with nonauxetic and auxetic configurations are considered in Figs. 8 and SM1.S11 (also refer to Figs. SM2.S9 to SM2.S12 of the supplementary material) to plot the in-plane constitutive behavior of C_{ij} elements with respect to angle ratio, (θ_3/θ_2 = 0.5 to 2) and multi-material ratio, (q= 1 to 2) under the axial, bending and shear mode of deformations. When the ratio of $\theta_3/\theta_2 = 1$, it indicates the symmetric multi-material case, as discussed in the preceding paragraphs. In-plane constitutive elements C_{11}, C_{22}, and C_{33} show increasing trends with the enhancement of q from 1 to 2 (33%, 26%, and 11% increament, respectively). However, C_{12}/C_{21} and C_{13}/C_{31} show a decreasing trend with respect to changing values of q from 1 to 2. Further C_{23} and C_{32} show increasing trends with up to 200 % variation with respect to variation in q from 1 to 2. The in-plane constitutive elements C_{ij} for auxetic asymmetric multi-material lattices show an increasing trend with the variation of q from 1 to 2.

We now explore the effect of variably-thickened cell walls in multimaterial lattices for non-auxetic and auxetic configurations. In Fig. SM1.S12, the non-dimensionalized values of elastic constitutive

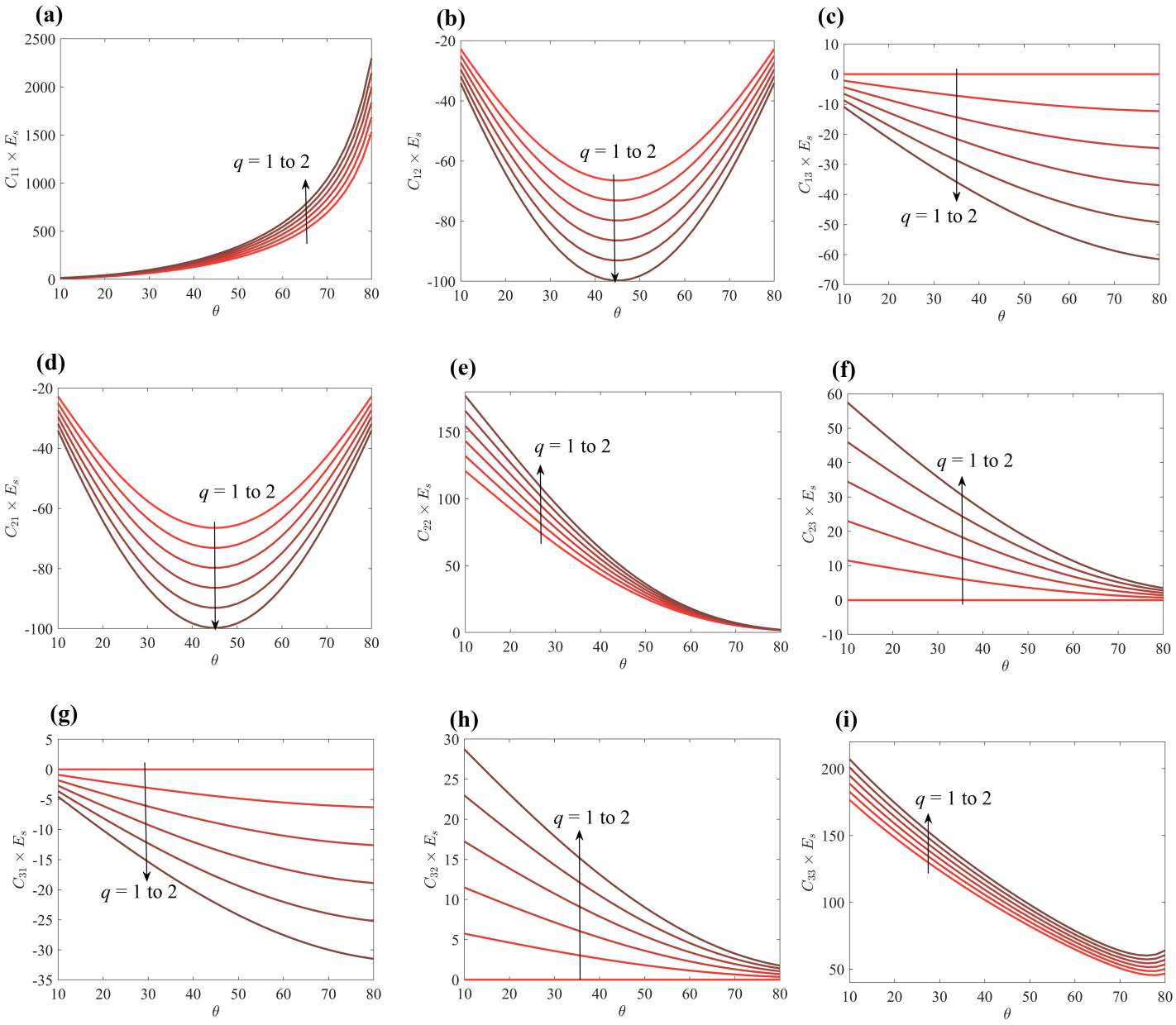

Figure 7: Complete in-plane constitutive (elastic modulus) matrix for non-auxetic symmetric multi-material honeycombs under axial, bending and shear effects. The non-dimensionalized value of elastic constitutive parameters for non-auxetic honeycombs ($E_1 = E_2 = qE_3 = E_s$, $L_1 = L_2 = L_3 = L = 1mm$, $t_1 = t_2 = t_3 = 0.2L$, $\eta_1 = \eta_2 = \eta_3 = 1$, and $\zeta_1 = \zeta_2 = \zeta_3 = 1$) are plotted for different cell angles under the consideration of axial, bending and shear deformations of cell walls. The variation of constitutive constants is plotted for different multi-material ratios (q =1 to 2). The normalization of the constitutive constants (C_{ij}) is carried out with respect to the intrinsic Young's modulus (E_s) of the vertical wall. Variations with respect to cell angle θ (in degree) are presented considering different values of q for **(a)** C_{11} **(b)** C_{12} **(c)** C_{13} **(d)** C_{21} **(e)** C_{22} **(f)** C_{23} **(g)** C_{31} **(h)** C_{32} **(i)** C_{33}. In these figures, the arrows depict the increasing trend of multi-material ratio (q) from lower ($q = 1$, which represents mono-material) to higher values ($q = 2$, which represents multi-material with higher ratio).

parameters (C_{ij}) are plotted for non-auxetic honeycombs ($E_1 = E_2 = qE_3 = E_s$, $L_1 = L_2 = L_3 = L = 1mm$, $t_1 = t_2 = t_3 = 0.2L$, $\eta_1 = \eta_2 = \eta_3 = \eta = 0.5$, and $\zeta_1 = \zeta_2 = \zeta_3 = \zeta = 1$ to 10, $q = 2$) considering different cell angles based on only bending deformations of cell walls. Further, the axial, and shear deformations are also considered along with the bending deformation of cell walls, and the

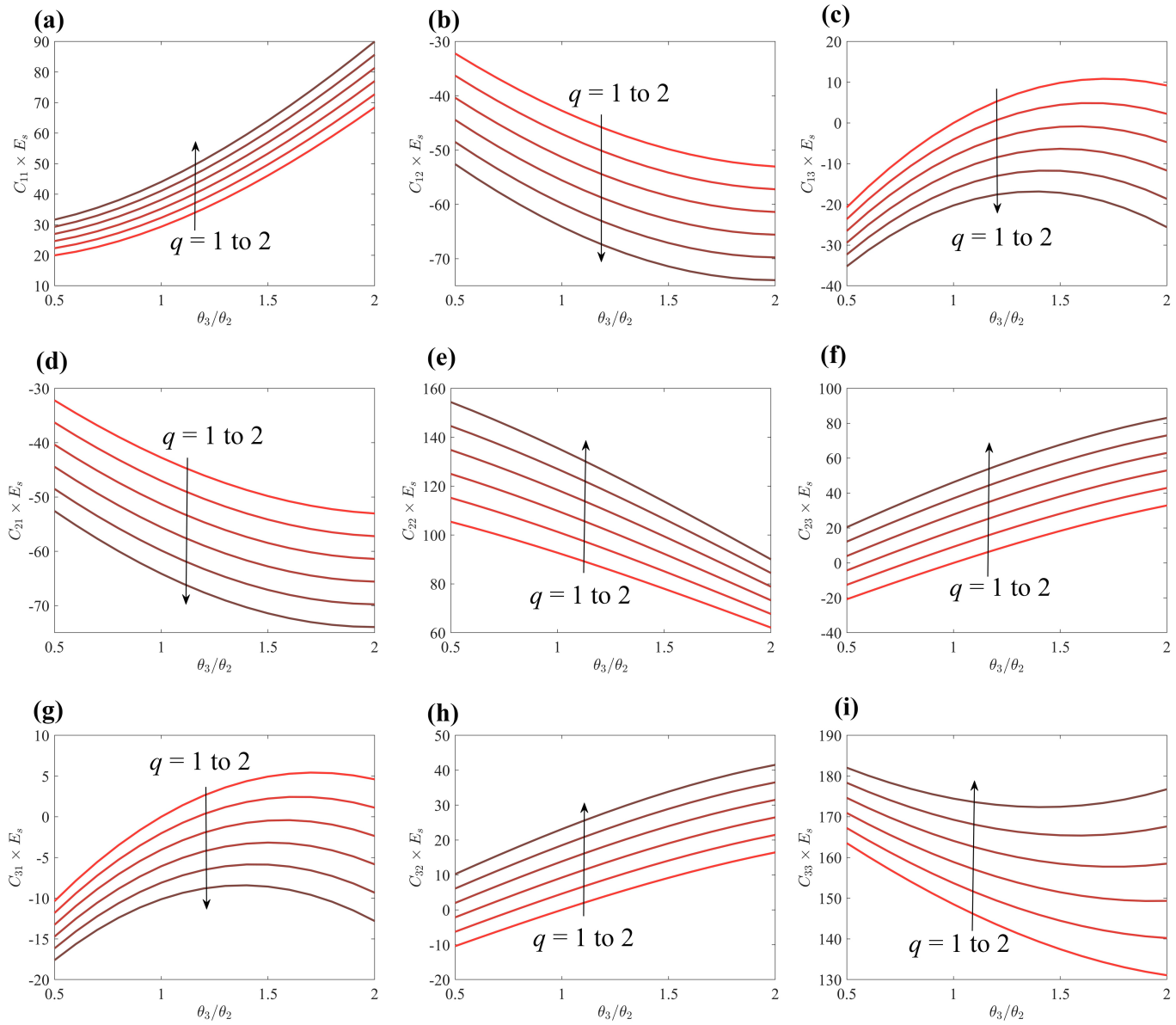

Figure 8: Complete in-plane constitutive (elastic modulus) matrix for nonauxetic asymmetric multi-material honeycombs under axial, bending and shear effects. The non-dimensionalized value of elastic constitutive parameters for nonauxetic honeycombs ($E_1 = E_2 = qE_3 = E_s$, $L_1 = L_2 = L_3 = L = 1mm$, $t_1 = t_2 = t_3 = 0.2L$, $\eta_1 = \eta_2 = \eta_3 = 1$, and $\zeta_1 = \zeta_2 = \zeta_3 = 1$) are plotted for angle ratio θ_3/θ_2 under the consideration of axial, bending and shear deformations of cell walls. The variation of constitutive constants is plotted for different multi-material ratios (q =1 to 2). The normalization of the constitutive constants (C_{ij}) is carried out with respect to the intrinsic Young's modulus (E_s) of the vertical wall. Variations with respect to angle ratio θ_3/θ_2 are presented considering different values of q for **(a)** C_{11} **(b)** C_{12} **(c)** C_{13} **(d)** C_{21} **(e)** C_{22} **(f)** C_{23} **(g)** C_{31} **(h)** C_{32} **(i)** C_{33}. In these figures, the arrows depict the increasing trend of multi-material ratio (q) from lower ($q = 1$, which represents mono-material) to higher values ($q = 2$, which represents multi-material with higher ratio).

corresponding elastic constitutive parameters are plotted in Fig. 9. In the supplementary material, additional results are presented for non-auxetic variably-thickened multimaterial lattices considering thinner and thicker cell walls with $t_1 = t_2 = t_3 = 0.1L, 0.3L$ (refer to Fig. SM2.S13 to SM2.S16). In these figures, the variation of constitutive constants is plotted for different ζ ratios (ζ =1 to 10), where ζ, the thickened-length ratio, represents the ratio of the length of thickened cell wall to the middle part

length. The cell wall thickness ratio (η) is taken as 0.5 ($\eta = 0.5$), which means that the thickness of the thicker part is double as compared to the middle part thickness of the walls. The normalization of the constitutive constants (C_{ij}) is carried out with respect to the intrinsic Young's modulus (E_s) of the vertical wall as before. It is observed that all the constitutive elastic constants can be modulated effectively by controlling length of the thickened cell wall. For C_{11}, C_{13}, and C_{31} the maximum effect of ζ is observed at higher cell wall angles, whereas for C_{12} and C_{21} the effect is maximum at cell wall angle 45°. On the other hand, effect of ζ on C_{22}, C_{23}, C_{32} and C_{33} is more prominent at lower cell wall angles. It can be noted that the contribution of considering the shear and axial deformations along with the bending deformation is significant on all the constitutive constants. The magnitude of constitutive constants increases by 10-20% (for $t/L = 0.1$), 15 to 30% (for $t/L = 0.2$), 30-45% (for $t/L = 0.3$) under the consideration of axial, shear and bending effect compared to the only bending case.

Similarly to explore the effect of variably-thickened cell walls on auxetic multi-material honeycombs, the in-plane constitutive behavior under different cell angles is plotted in Fig. SM1.S13 considering only bending ($t/L = 0.2$). To asses the effect of shear and axial effect along with bending, a similar variation is presented in Fig. SM1.S14 for $t/L = 0.2$. Further, we have explored the variably-thickened auxetic multi-material honeycombs considering thinner and thicker cell walls with $t/L = 0.1, 0.3$ (Figs. SM2.S17 - SM2.S20 in the supplementary material). It is observed variably-thickened cell wall length significantly affects all the in-plane constitutive matrix elements depending on the cell wall angle. In the auxetic case, the effect of ζ on C_{11}, C_{12}, C_{21} and C_{22} is more prominent at cell wall angle 45°. The maximum effect of ζ for all other constitutive elastic constants is observed at a higher cell wall angle. It is noted that the consideration of axial and shear deformation significantly affects the magnitude of each constitutive element. It is also worth noting here that the effect of variably-thickened cell walls (ζ) for both regular and auxetic honeycombs becomes more prominent when its value increases from 1 to 5 and this effect gradually becomes less as its value further increases from 5 to 10. Such observations can play an important role in achieving optimized properties by controlling the variably-thickened beam-level architecture in multi-material honeycomb lattices.

After investigating symmetric lattices, we have presented results for variably-thickened cell walls considering asymmetric multi-material nonauxetic and auxetic lattices (Figs. 10, SM1.S15, and SM2.S21 - SM2.S24). It can be noted, when θ_3/θ_2 is equivalent to 1, then the variation of C_{ij} elements becomes similar to regular symmetric multi-material honeycombs, as discussed in the preceding paragraphs. The C_{ij} elements are plotted for asymmetric designs concerning ζ and angle ratio θ_3/θ_2, wherein an intricate interplay among the prospective design parameters can be noticed that would lead to important insights

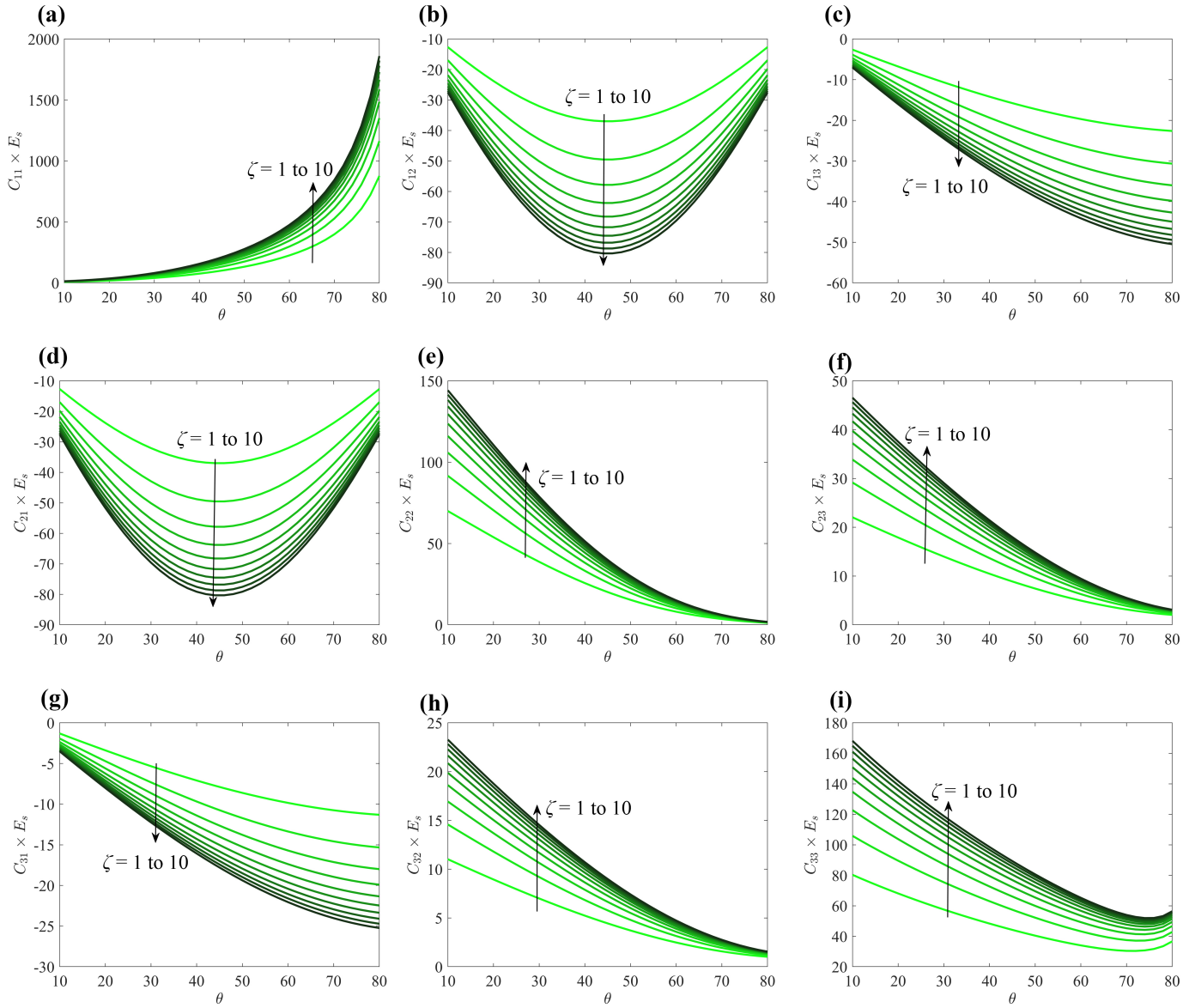

Figure 9: Complete in-plane constitutive (elastic modulus) matrix for non-auxetic multi-material symmetric variably-thickened cell wall honeycombs under bending, axial and shear effects. The non-dimensionalized values of elastic constitutive parameters for non-auxetic honeycombs ($E_1 = E_2 = qE_3 = E_s$, $L_1 = L_2 = L_3 = L = 1mm$, $t_1 = t_2 = t_3 = 0.2L$, $\eta_1 = \eta_2 = \eta_3 = \eta = 0.5$, and $\zeta_1 = \zeta_2 = \zeta_3 = \zeta = 1$ to 10, $q = 2$) are plotted for different cell angles under the consideration of bending, axial and shear deformations of cell walls. The variation of constitutive constants is plotted for different ζ ratios (ζ =1 to 10). Here, ζ represents a ratio of the length of the thickened portion near the joint to the less-thick middle part. The cell wall thickness ratio (η) is considered as 0.5 ($\eta = 0.5$), which represents that the thickness near the end part is double as compared to the middle part thickness. The normalization of the constitutive constants (C_{ij}) is carried out with respect to the intrinsic Young's modulus (E_s) of the vertical wall. Variations with respect to cell angle θ (in degree) considering different values of ζ are presented for **(a)** C_{11} **(b)** C_{12} **(c)** C_{13} **(d)** C_{21} **(e)** C_{22} **(f)** C_{23} **(g)** C_{31} **(h)** C_{32} **(i)** C_{33}. In these figures, the arrows depict the increasing trend of ζ from lower ($\zeta = 1$, which represents that the length of the thickened part is equal to middle part) to higher values ($\zeta = 10$, which represents that the length of the thickened part is 1/10 of the middle part).

for developing multifunctional lightweight architected materials.

The effect of another parameter in variably-thickened cell walls, η indicating the cell wall thickness ratio (refer to Fig. 3(b)), is studied further on multi-material ($q = 2$) non-auxetic and auxetic honeycombs ($\zeta_1 = \zeta_2 = \zeta_3 = \zeta = 1$). In Fig. 11 and SM1.S16 to SM1.S18 (also refer to Figs. SM2.S25

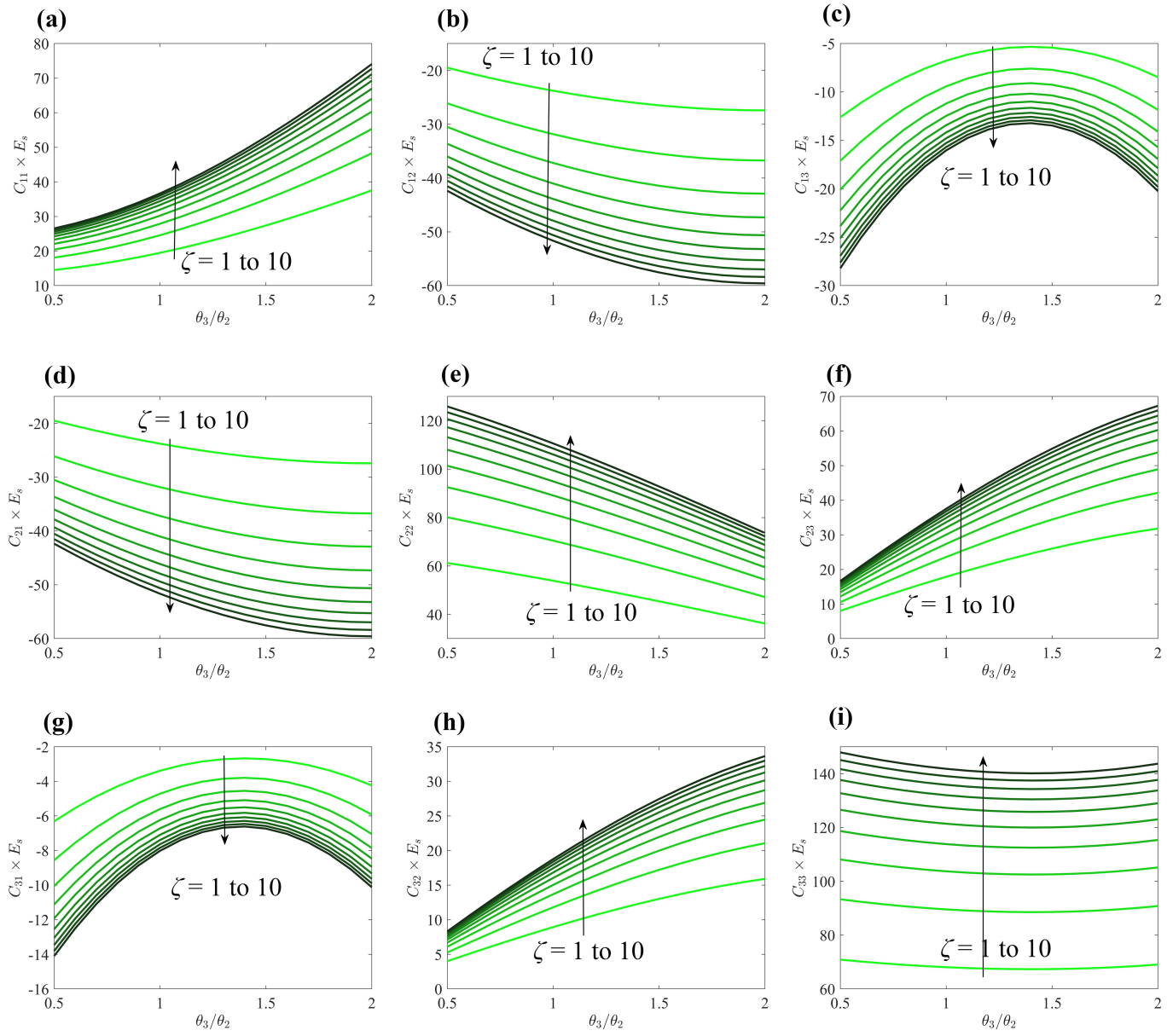

Figure 10: Complete in-plane constitutive (elastic modulus) matrix for nonauxetic asymmetric multi-material variably-thickened cell wall honeycombs under axial, bending and shear effects. The non-dimensionalized values of elastic constitutive parameters for non-auxetic honeycombs ($E_1 = E_2 = qE_3 = E_s$, $L_1 = L_2 = L_3 = L = 1mm$, $t_1 = t_2 = t_3 = 0.2L$, $\eta_1 = \eta_2 = \eta_3 = \eta = 0.5$, and $\zeta_1 = \zeta_2 = \zeta_3 = \zeta$ = 1 to 10, $q = 2$) are plotted for different cell angle ratios θ_3/θ_2 under the consideration of bending, axial and shear deformations of cell walls. The variation of constitutive constants is plotted for different ζ ratios (ζ =1 to 10). Here, ζ represents a ratio of the length of the thickened portion near the joint to the less-thick middle part. The cell wall thickness ratio (η) is considered as 0.5 ($\eta = 0.5$), which represents that the thickness near the end part is double as compared to the middle part thickness. The normalization of the constitutive constants (C_{ij}) is carried out with respect to the intrinsic Young's modulus (E_s) of the vertical wall. Variations with respect to angle ratio θ_3/θ_2 considering different values of ζ are presented for **(a)** C_{11} **(b)** C_{12} **(c)** C_{13} **(d)** C_{21} **(e)** C_{22} **(f)** C_{23} **(g)** C_{31} **(h)** C_{32} **(i)** C_{33}. In these figures, the arrows depict the increasing trend of ζ from lower ($\zeta = 1$, which represents that the length of the thickened part is equal to middle part) to higher values ($\zeta = 10$, which represents that the length of the thickened part is 1/10 of the middle part).

to SM2.S32 of the supplementary material), the elastic constitutive constants (C_{ij}) are plotted for multi-material regular (non-auxetic) and auxetic honeycomb structures by considering different η val-

ues ($\eta_1 = \eta_2 = \eta_3 = \eta = 0.5$ to 1). In these figures, the arrows depict the increasing trend of cell wall thickness ratio (η) from $\eta = 0.5$ (which represents the thickness of cell wall is double near the joints compared to the middle part) to $\eta = 1$ (which represents the thickness of cell wall is same near the joints compared to the middle part). In Fig. SM1.S16, the non-dimensionalized value of elastic constitutive constants (C_{ij}) for non-auxetic honeycombs ($E_1 = E_2 = qE_3 = E_s$, $L_1 = L_2 = L_3 = L = 1mm$, $t_1 = t_2 = t_3 = 0.2L$ and $\zeta_1 = \zeta_2 = \zeta_3 = \zeta = 1$, $q = 2$) is plotted at different cell angles (θ) under the consideration of bending deformation of cell walls. Similarly, the non-dimensionalized value of elastic constitutive constants (C_{ij}) for non-auxetic honeycomb is plotted in Fig. 11 at different cell angles (θ) under the consideration of combined axial, shear and bending deformations of cell walls. For a more comprehensive analysis, the similar variations of in-plane constitutive constants for thinner-walled and thicker-walled non-auxetic multi-material honeycombs are presented in the supplementary material (refer to Figs. SM2.S25 to SM2.S28). It is observed that all the elastic constitutive constants (C_{ij}) are significantly affected by η. The magnitude of elastic constitutive constants (C_{ij}) increases by approximately 3 to 4 times as the value of η increases from 0.5 to 1. It is noted that the effect of η on C_{11}, C_{13} and C_{31} is more prominent when the cell wall angle is more than 60°, whereas this effect for C_{12} and C_{21} is maximum at cell wall angle 45°. The effect of η on C_{22}, C_{23}, C_{32} and C_{33} is comparatively high at lower cell wall angles. From the figures, it can also be noted that the consideration of axial and shear deformations of cell walls plays a significant role in the characterization of constitutive constants (C_{ij}). The elastic constitutive constants (C_{ij}) under axial, shear and bending effects become 20-30% more than the only bending case. In Fig. SM1.S17 and SM1.S18, the non-dimensionalized value of elastic constitutive constants (C_{ij}) for auxetic honeycombs ($E_1 = E_2 = qE_3 = E_s$, $L_1 = L_2 = L_3 = L = 1mm$, $t_1 = t_2 = t_3 = 0.2L$ and $\zeta_1 = \zeta_2 = \zeta_3 = \zeta = 1$, $q = 2$) is plotted at different cell angle (θ) under consideration of only bending deformations and the combined effect of axial, shear and bending deformations. For a more comprehensive analysis, the variation of elastic constitutive constants is presented further considering thinner and thicker walled honeycombs in the supplementary material (refer to Figs. SM2.S29 to SM2.S32). It is noted that the effect of η on C_{11}, C_{12} and C_{21} is more prominent when the cell wall angle is 45°, whereas this effect for C_{22} is maximum at cell wall angle in the range of 10° to 40°. The effect of η on C_{13}, C_{31}, C_{23}, C_{32} and C_{33} is significantly high at lower cell wall angles.

Subsequently, the effect of cell wall thickness ratio η is studied for asymmetric multi-material nonauxetic and auxetic honeycombs in Fig. 12, and SM1.S19 (also refer to Figs. SM2.S33 to SM2.S36). The in-plane constitutive constants are plotted with respect to η and cell angle ratio θ_3/θ_2. It can be noted that when the ratio of θ_3/θ_2 is equivalent to 1, the results obtained are similar to the symmetric case

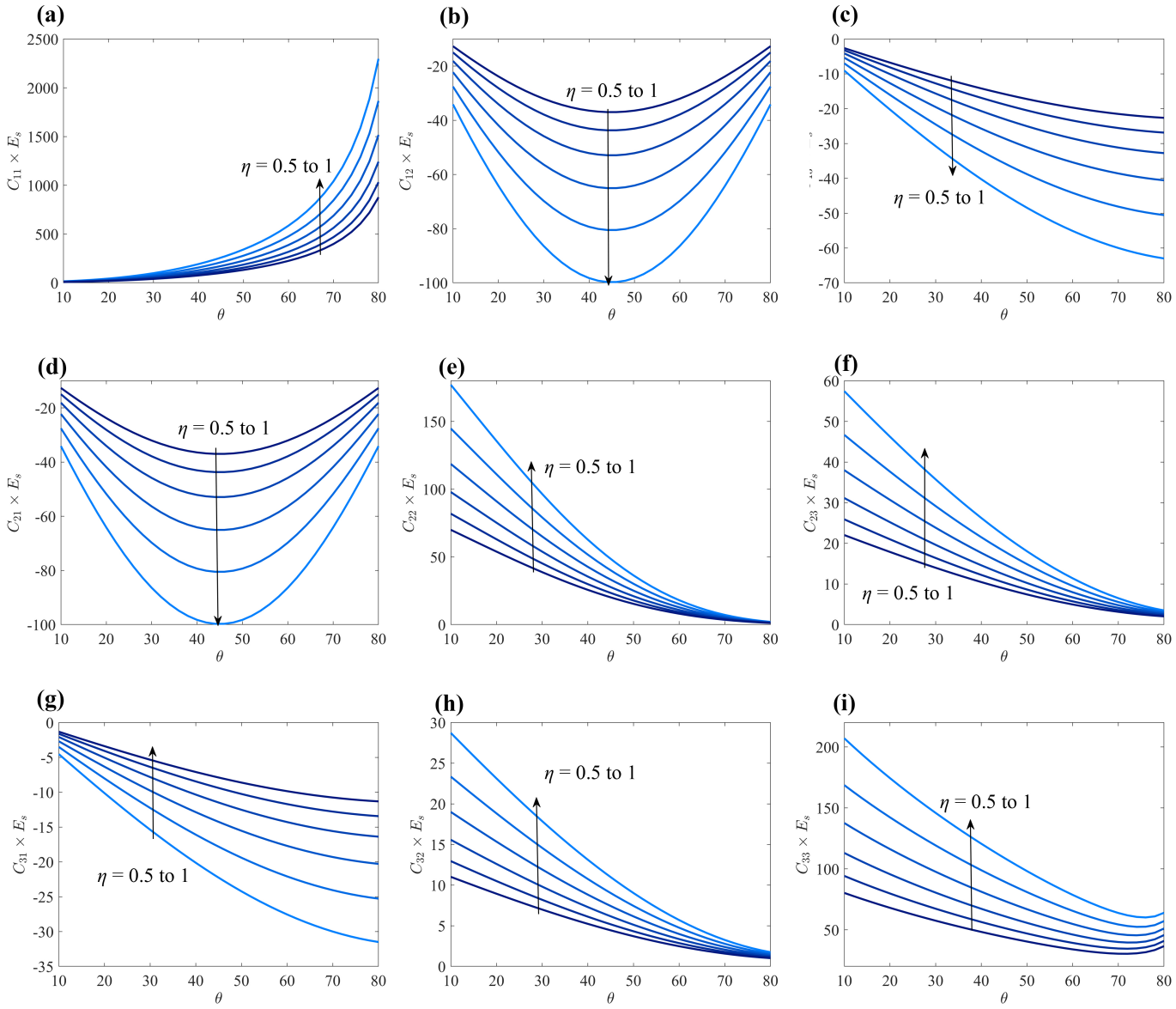

Figure 11: Effect of variably-thickened cell wall thickness ratio (η) on complete in-plane constitutive (elastic modulus) matrix for non-auxetic multi-material symmetric honeycombs under bending, axial and shear deformations. The non-dimensionalized values of elastic constitutive parameters for non-auxetic honeycombs ($E_1 = E_2 = qE_3 = E_s$, $L_1 = L_2 = L_3 = L = 1mm$, $t_1 = t_2 = t_3 = 0.2L$, $\eta_1 = \eta_2 = \eta_3 = \eta = 0.5$ to 1, and $\zeta_1 = \zeta_2 = \zeta_3 = \zeta = 1$, $q = 2$) are plotted for different cell angles under the consideration of bending, axial and shear deformation of cell walls. The variation of constitutive constants is plotted for different η ratios ($\eta = 0.5$ to 1) considering $\zeta = 1$. The normalization of the constitutive constants (C_{ij}) is carried out with respect to the intrinsic Young's modulus (E_s) of the vertical wall. Variations with respect to cell angle θ (in degree) considering different values of η are presented for **(a)** C_{11} **(b)** C_{12} **(c)** C_{13} **(d)** C_{21} **(e)** C_{22} **(f)** C_{23} **(g)** C_{31} **(h)** C_{32} **(i)** C_{33}. In these figures, the arrows depict the increasing trend of cell wall thickness ratio (η) from lower (0.5, which represents that the thickness of cell walls is twice near the joints compared to the middle part) to higher values ($\eta = 1$, which represents that the thickness of the cell walls is uniform throughout the length).

of nonauxetic and auxetic lattices. With the introduction of asymmetry in the geometry, an intricate interplay among the prospective design parameters can be noticed that would lead to important insights for developing multifunctional lightweight architected materials in an expanded design space.

The effect of wall thickness corresponding to the middle part of a variably-thickened cell wall (indi-

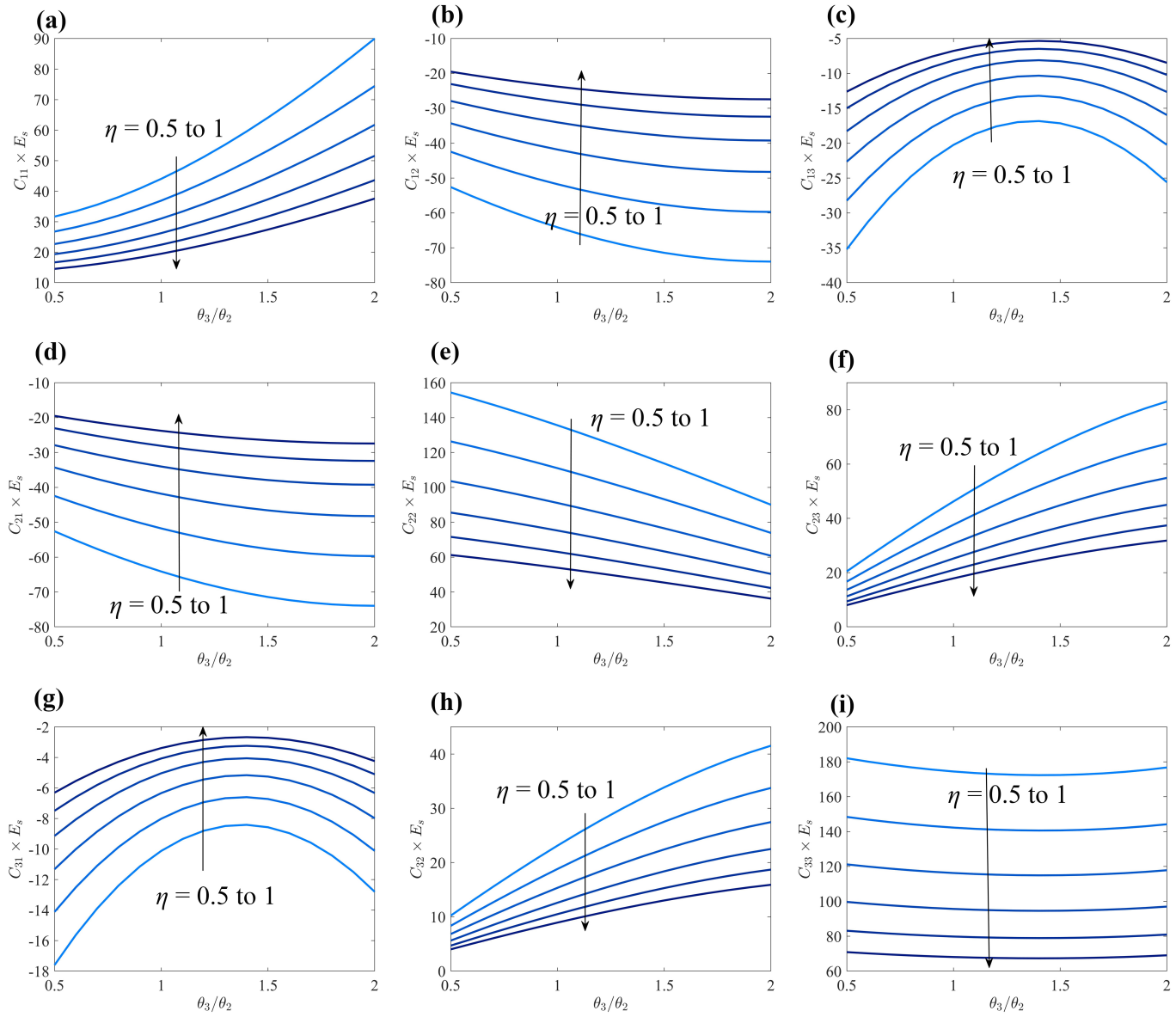

Figure 12: Effect of variably-thickened cell wall thickness ratio (η) on complete in-plane constitutive (elastic modulus) matrix for nonauxetic asymmetric multi-material honeycombs under axial, bending and shear effect. The non-dimensionalized values of elastic constitutive parameters for nonauxetic honeycombs ($E_1 = E_2 = qE_3 = E_s$, $L_1 = L_2 = L_3 = L = 1mm$, $t_1 = t_2 = t_3 = 0.2L$, $\eta_1 = \eta_2 = \eta_3 = \eta = 0.5$ to 1, and $\zeta_1 = \zeta_2 = \zeta_3 = \zeta = 1$, $q = 2$) are plotted with the angle ratio θ_3/θ_2 under the consideration of bending, axial and shear deformations of cell walls. The variation of constitutive constants is plotted for different η ratios ($\eta = 0.5$ to 1) with $\zeta = 1$. The normalization of the constitutive constants (C_{ij}) is carried out with respect to the intrinsic Young's modulus (E_s) of the vertical wall. Variations with respect to angle ratio θ_3/θ_2 considering different values of η are presented for **(a)** C_{11} **(b)** C_{12} **(c)** C_{13} **(d)** C_{21} **(e)** C_{22} **(f)** C_{23} **(g)** C_{31} **(h)** C_{32} **(i)** C_{33}. In these figures, the arrows depict the increasing trend of cell wall thickness ratio (η) from lower (0.5, which represents that the thickness of cell walls is twice near the joints compared to the middle part) to higher values ($\eta = 1$, which represents that the thickness of the cell walls is uniform throughout the length).

cated as t_{ih} in Fig 3(b); note that we have dropped the subscript in most discussions in this section as thickness of all the three members are taken as same) is studied further on the in-plane constitutive behavior of multi-material ($\zeta_1 = \zeta_2 = \zeta_3 = \zeta = 5$, $\eta_1 = \eta_2 = \eta_3 = \eta = 0.5$, $q = 2$) non-auxetic and auxetic honeycombs. In Fig. 13, and SM1.S20 to SM1.S22, the elastic constitutive constants (C_{ij}) are investigated considering different thickness of cell walls ($t = 0.06L$ to $t = 0.2L$, ranging from thin to moderately

thick). Such an analysis would further emphasize the importance of considering shear and axial beam-level deformations for thicker cell wall honeycombs. In Fig. SM1.S20, the non-dimensionalized value of elastic constitutive constants (C_{ij}) for thin to thick-walled non-auxetic multi-material honeycombs ($E_1 = E_2 = qE_3 = E_s$, $L_1 = L_2 = L_3 = L = 1mm$, $\eta_1 = \eta_2 = \eta_3 = \eta = 0.5$, and $\zeta_1 = \zeta_2 = \zeta_3 = \zeta = 5$, $q = 2$) are plotted for different cell angles under the consideration of only bending deformations of cell walls. Similarly, the non-dimensionalized value of elastic constitutive constants (C_{ij}) for thin to thick-walled non-auxetic honeycomb is plotted in Fig. 13 at different cell angles by consideration of axial, shear and bending deformations of cell walls. It is observed that all the in-plane elastic constitutive constants (C_{ij}) are significantly affected by the thickness of cell walls (t). In general, the magnitude of elastic constitutive constants (C_{ij}) decreases significantly as the value of the thickness of cell walls (t) increases from 0.06 to 0.2. It is noted that the effect of cell wall thickness on C_{11}, C_{13} and C_{31} becomes more prominent as the cell wall angle increases, whereas this effect on C_{12} and C_{21} is maximum at cell wall angle 45°. Similarly, the effect of cell wall thickness t on C_{22}, C_{23}, C_{32} and C_{33} decrease as the cell wall angle approaches higher values. From Fig. SM1.S20 and 13, it can be noted that the in-plane constitutive constants (C_{ij}) for thin-walled honeycomb is not affected much by considering the of axial and shear deformations of cell walls. The influence of axial and shear deformations becomes higher in the case of thicker cell walls. In Fig. SM1.S21, the non-dimensionalized value of elastic constitutive constants (C_{ij}) for thin to thick-walled auxetic multi-material honeycombs ($E_1 = E_2 = qE_3 = E_s$, $L_1 = L_2 = L_3 = L = 1mm$, $\eta_1 = \eta_2 = \eta_3 = \eta = 0.5$, and $\zeta_1 = \zeta_2 = \zeta_3 = \zeta = 5$, $q = 2$) is plotted at different cell angles (θ) under the consideration of only bending deformations of cell walls. Further, the additional effect of shear and axial deformations in the case of auxetic honeycombs is included in Fig. SM1.S22. In multi-material auxetic honeycombs, it is noted that the effect of wall thickness on C_{11}, C_{12} and C_{21} is more prominent when cell wall angle is around 45°, whereas this effect of wall thickness on C_{22} is maximum for cell wall angle between 10° to 40°. Similarly, the effect of wall thickness on C_{13}, C_{31}, C_{23}, C_{32} and C_{33} becomes prominent as the cell wall angle increases.

The effect of wall thickness is further explored for nonauxetic and auxetic configurations of the asymmetric multi-material lattices, as shown in Figs. 14 and SM1.S23. Here, if the angle ratio θ_3/θ_2 is considered as 1, then the results are obtained same as symmetric multi-material nonauxetic and auxetic configurations. In general, increasing cell wall thickness leads to a lesser value of the constitutive constants, while there exists an interesting interplay among the other design parameters for developing multifunctional optimized lattice configurations.

To understand the interplay among unit cell geometry in terms of side wall lengths, cell angles and

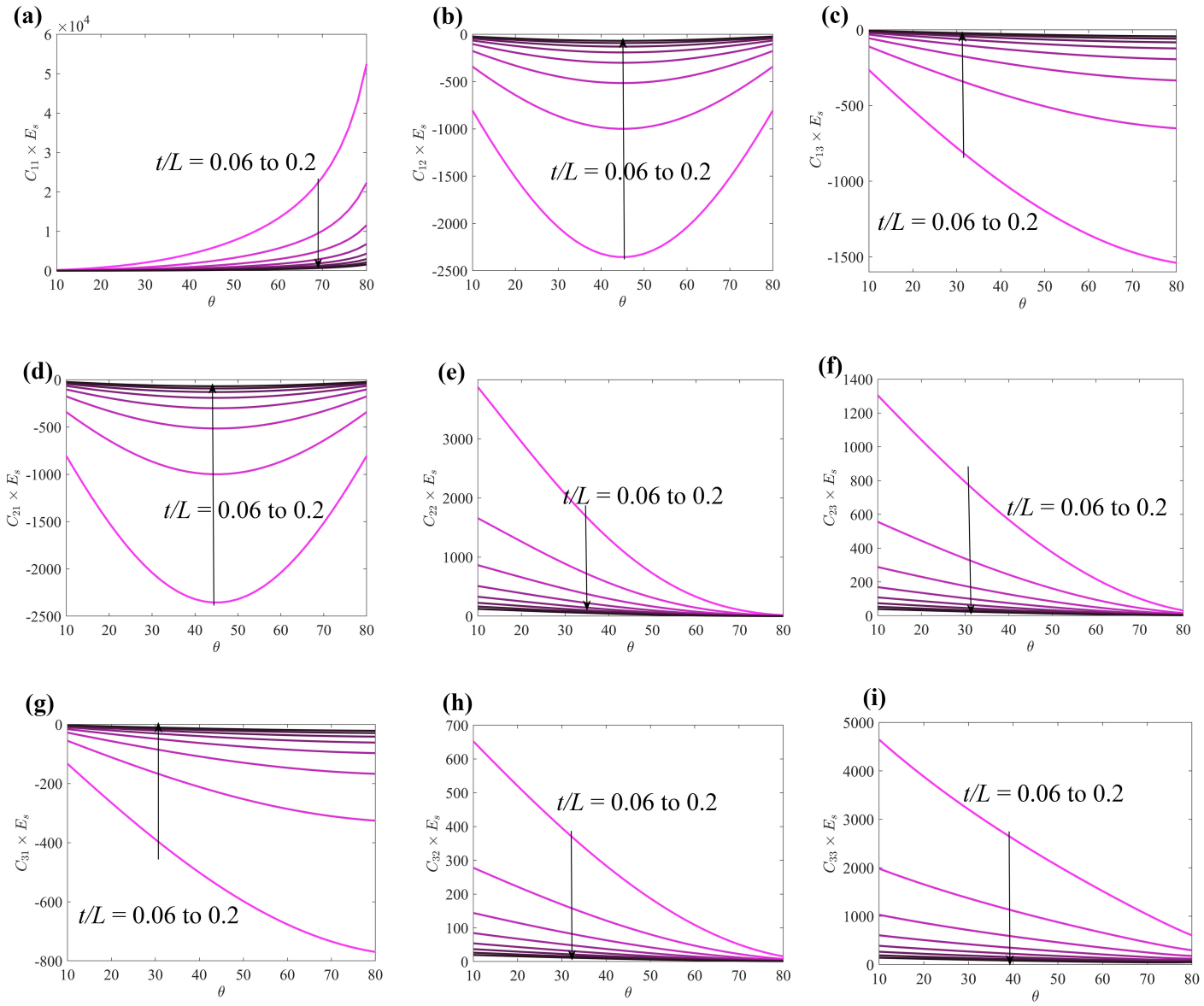

Figure 13: Effect of wall thickness on complete in-plane constitutive (elastic modulus) matrix for non-auxetic multi-material variably-thickened cell wall symmetric honeycombs under bending, axial and shear deformations. The non-dimensionalized values of elastic constitutive parameters for thin to thick-walled non-auxetic honeycombs ($E_1 = E_2 = qE_3 = E_s$, $L_1 = L_2 = L_3 = L = 1mm$, $\eta_1 = \eta_2 = \eta_3 = \eta = 0.5$, and $\zeta_1 = \zeta_2 = \zeta_3 = \zeta = 5$, $q = 2$) are plotted considering different cell angles under bending, axial and shear deformations of cell walls. The variation of constitutive constants is plotted for different wall thicknesses to length ratio t/L, thin (t=0.06L) to thick (t=0.2L) with $\eta = 0.5$ and $\zeta = 5$. The normalization of the constitutive constants (C_{ij}) is carried out with respect to the intrinsic Young's modulus (E_s) of the vertical wall. Variations with respect to cell angle θ (in degree) considering different values of t/L are presented for **(a)** C_{11} **(b)** C_{12} **(c)** C_{13} **(d)** C_{21} **(e)** C_{22} **(f)** C_{23} **(g)** C_{31} **(h)** C_{32} **(i)** C_{33}. In these figures, the arrows depict the increasing trend of thickness (t/L) from lower to higher values.

multimaterial parameters along with beam-level architectures, the effect of vertical wall length to slant walls length ratio (H/L) on the effective elastic properties of honeycomb is studied for variably-thickened multi-material non-auxetic and auxetic honeycombs ($E_1 = E_2 = qE_3 = E_s$, $L_1 = L_2 = L_3 = L = 1mm$, $t_1 = t_2 = t_3 = 0.2L$, $\eta_1 = \eta_2 = \eta_3 = \eta = 0.5$, and $\zeta_1 = \zeta_2 = \zeta_3 = \zeta = 5$, $q = 2$). In Fig. 15, and SM1.S24 to SM1.S26, the elastic constitutive constants (C_{ij}) are presented for different H/L values

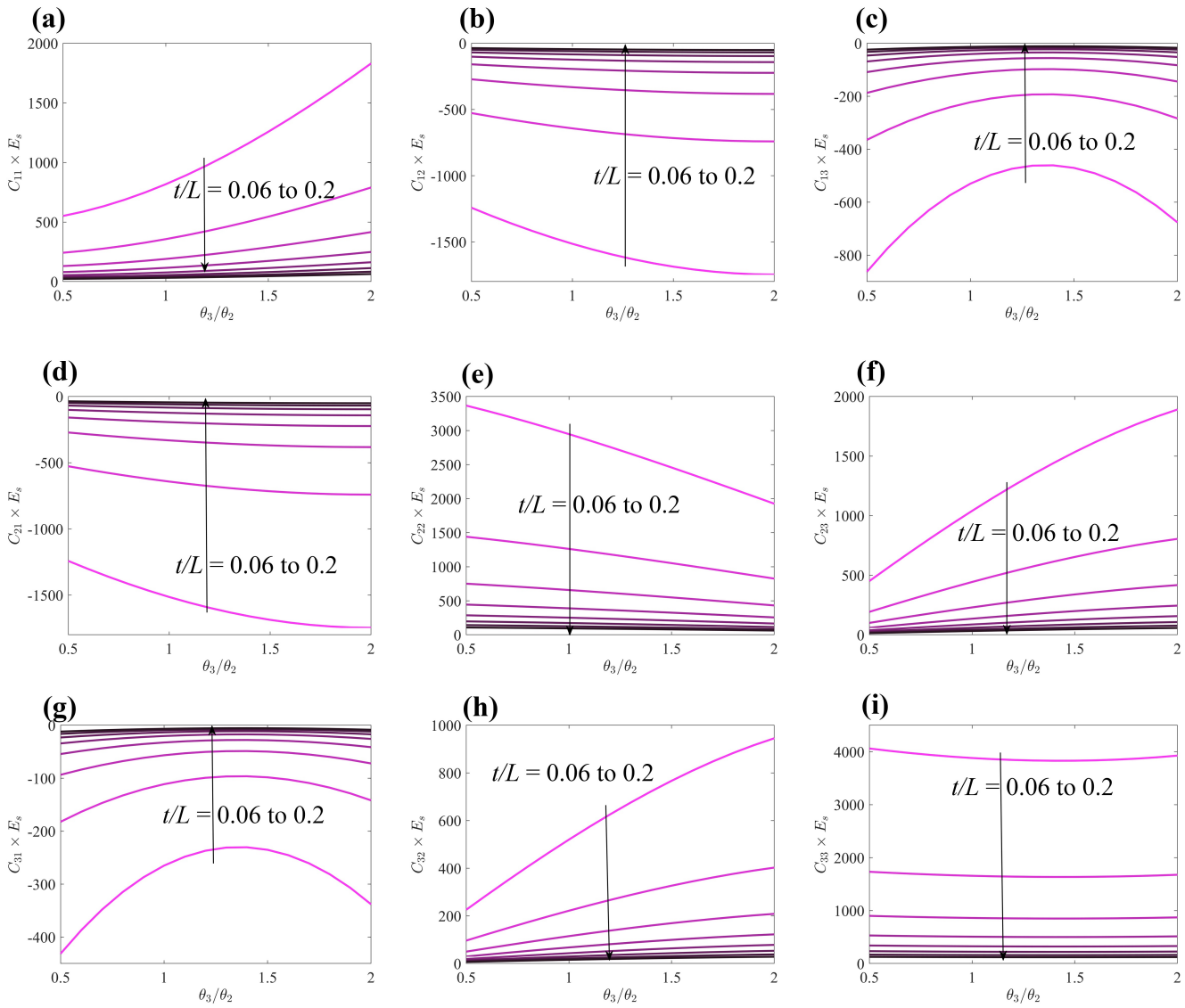

Figure 14: Effect of cell wall thickness on complete in-plane constitutive (elastic modulus) matrix for non-auxetic asymmetric multi-material variably-thickened cell wall honeycombs under axial, bending and shear effects. The non-dimensionalized values of elastic constitutive parameters for thin to thick-walled nonauxetic honeycombs ($E_1 = E_2 = qE_3 = E_s$, $L_1 = L_2 = L_3 = L = 1mm$, $t_1 = t_2 = t_3 = 0.2L$, $\eta_1 = \eta_2 = \eta_3 = \eta = 0.5$, and $\zeta_1 = \zeta_2 = \zeta_3 = \zeta = 5$, $q = 2$) are plotted with cell angle ratios θ_3/θ_2 under the consideration of axial, bending and shear deformations of cell walls. The variation of constitutive constants is plotted for different wall thicknesses to length ratio t/L, thin (t=$0.06L$) to thick (t=$0.2L$), with $\eta = 0.5$ and $\zeta = 5$. The normalization of the constitutive constants (C_{ij}) is carried out with respect to the intrinsic Young's modulus (E_s) of the vertical wall. Variations with respect to angle ratio θ_3/θ_2 considering different values of t/L are presented for **(a)** C_{11} **(b)** C_{12} **(c)** C_{13} **(d)** C_{21} **(e)** C_{22} **(f)** C_{23} **(g)** C_{31} **(h)** C_{32} **(i)** C_{33}. In these figures, the arrows depict the increasing trend of thickness (t/L) from lower to higher values.

considering $t_1 = t_2 = t_3 = 0.2L$, ranging from 1 to 1.5 (non-auxetic configurations). Figs. SM2.S37 to SM2.S40 in the supplementary material elaborate the variation of in-plane constitutive constants for relatively thinner-walled and thicker-walled non-auxetic configurations. In Fig. SM1.S24, the non-dimensionalized elastic constitutive constants (C_{ij}) for non-auxetic variably-thickened multi-material honeycombs are plotted for different H/L ratios under different cell angle by considering only bending

deformations of cell walls. Similarly, the non-dimensionalized value of elastic constitutive constants (C_{ij}) for non-auxetic honeycombs with different H/L ratios is plotted in Fig. 15 at different cell angles by considering the axial, shear and bending deformations of cell walls. It is observed that all the elastic constitutive constants (C_{ij}) are significantly affected by H/L ratio. The effect of H/L ratio on C_{11}, C_{13} and C_{31} becomes more prominent at higher cell wall angles, whereas its effect on C_{22}, C_{23}, C_{32} and C_{33} is maximum when cell wall angle is smaller. Similarly, effect of H/L ratio on C_{12} and C_{21} is maximum at the cell wall angle of 45°. It can further be noted that the contribution of the shear and axial deformation effect is significant on all the constitutive constants. The magnitude of all in-plane constitutive constants is 10 to 15% higher under the consideration of axial, shear and bending effects compared to thr only bending case.

Fig. SM1.S25 shows the variation C_{ij} of auxetic variably-thickened multi-material honeycombs ($E_1 = E_2 = qE_3 = E_s$, $L_1 = H = 1$ to 1.5mm, $L_2 = L_3 = L = 1$mm, $t_1 = t_2 = t_3 = 0.2L$, $\eta_1 = \eta_2 = \eta_3 = \eta = 0.5$, and $\zeta_1 = \zeta_2 = \zeta_3 = \zeta = 5$, $q = 2$) for different H/L ratios and cell angles under the consideration of only bending deformations of cell walls. Such variation for auxetic variably-thickened multi-material honeycombs is also plotted in Fig. SM1.S26 under the combined effect of axial, shear and bending deformations. For a more comprehensive analysis, the variation of in-plane constitutive constants for thinner-walled and thicker-walled variably-thickened auxetic multi-material honeycombs considering different H/L values is further elaborated in the supplementary material (refer to Figs. SM2.S41 to SM2.S44). From the numerical results, it is noted that the effect of H/L ratio on C_{11}, C_{13}, C_{31} and C_{33} becomes more prominent as the cell wall angle increases, whereas the effect of H/L ratio on C_{12}, C_{21} and C_{22} is maximum for cell wall angle at 45°. Similarly, the effect of H/L ratio on C_{23} and C_{32} is maximum when the cell wall angle is in the range of 40° to 60°. The effect of H/L ratio on C_{12} and C_{21} is found to be maximum at the cell wall angle of 45°. From the comparative results of different cell wall thicknesses, it becomes evident that the effect of axial and shear deformation becomes more significant for thicker-walled honeycombs.

The effect of the vertical wall-to-slant wall-length ratio (H/L) is studied further for asymmetric multi-material nonauxetic and auxetic cases (refer to Fig. 16, SM1.S27, and SM2.S45 to SM2.S48). It can be noted here that when the value of angle ratio θ_3/θ_2 equals 1, the results are similar to symmetric multi-material nonauxetic and auxetic configurations. In general, we show that the proposed bi-level design space, including unit cell level geometric parameters such as a cell wall angles constituting asymmetry in the hexagonal units, cell wall (multi-)material properties, thickness and dimensions along with beam level architecture, can lead to optimum design of multi-functional metamaterials. In this context, it may

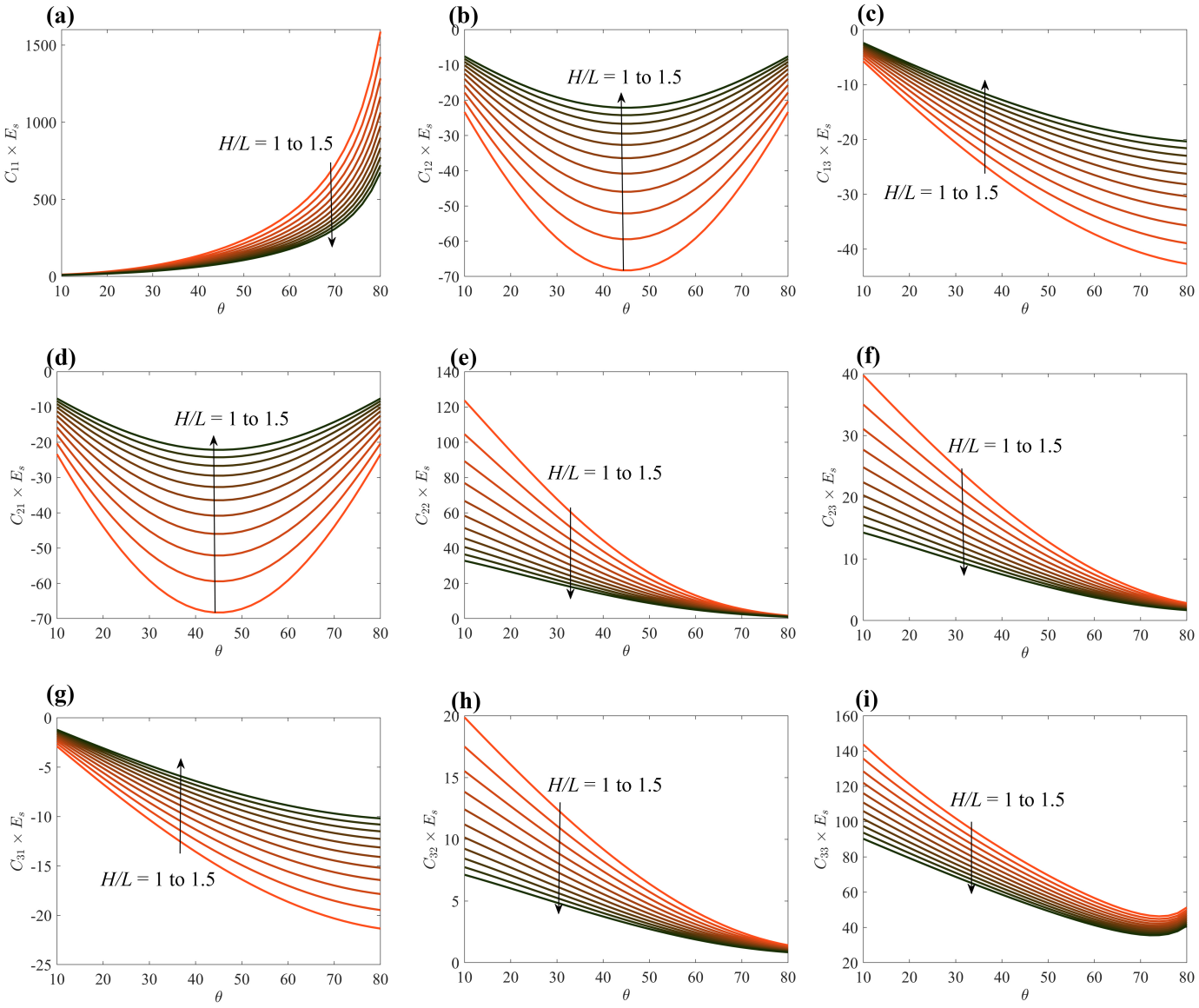

Figure 15: Effect of H/L ratio (ratio of the length of vertical and slant walls) on the complete in-plane constitutive (elastic modulus) matrix for non-auxetic multi-material variably-thickened cell wall symmetric honeycombs under bending, axial and shear deformations. The non-dimensionalized values of elastic constitutive parameters for non-auxetic honeycombs ($E_1 = E_2 = qE_3 = E_s$, $L_1 = H = 1$ to 1.5mm, $L_2 = L_3 = L = 1$mm, $t_1 = t_2 = t_3 = 0.2L$, $\eta_1 = \eta_2 = \eta_3 = \eta = 0.5$, and $\zeta_1 = \zeta_2 = \zeta_3 = \zeta = 5$, $q = 2$) are plotted for different cell angles under the consideration of bending, axial and shear deformations of cell walls. The variation of constitutive constants is plotted for different H/L values with $\eta = 0.5$ and $\zeta = 5$. The normalization of the constitutive constants (C_{ij}) is carried out with respect to the intrinsic Young's modulus (E_s) of the vertical wall. Variations with respect to cell angle θ (in degree) considering different values of H/L are presented for **(a)** C_{11} **(b)** C_{12} **(c)** C_{13} **(d)** C_{21} **(e)** C_{22} **(f)** C_{23} **(g)** C_{31} **(h)** C_{32} **(i)** C_{33}. In these figures the arrows depict an increasing trend of H/L from $H/L = 1$ to $H/L = 1.5$.

be noted that the design space can be significantly expanded further by considering different values of t_i, ζ_i and η_i for the three cell walls ($i = 1, 2, 3$). In addition, a range of other symmetric and asymmetric architectures can be introduced at the beam level. Such results can be directly obtained (or with slight modifications) following the proposed analytical framework.

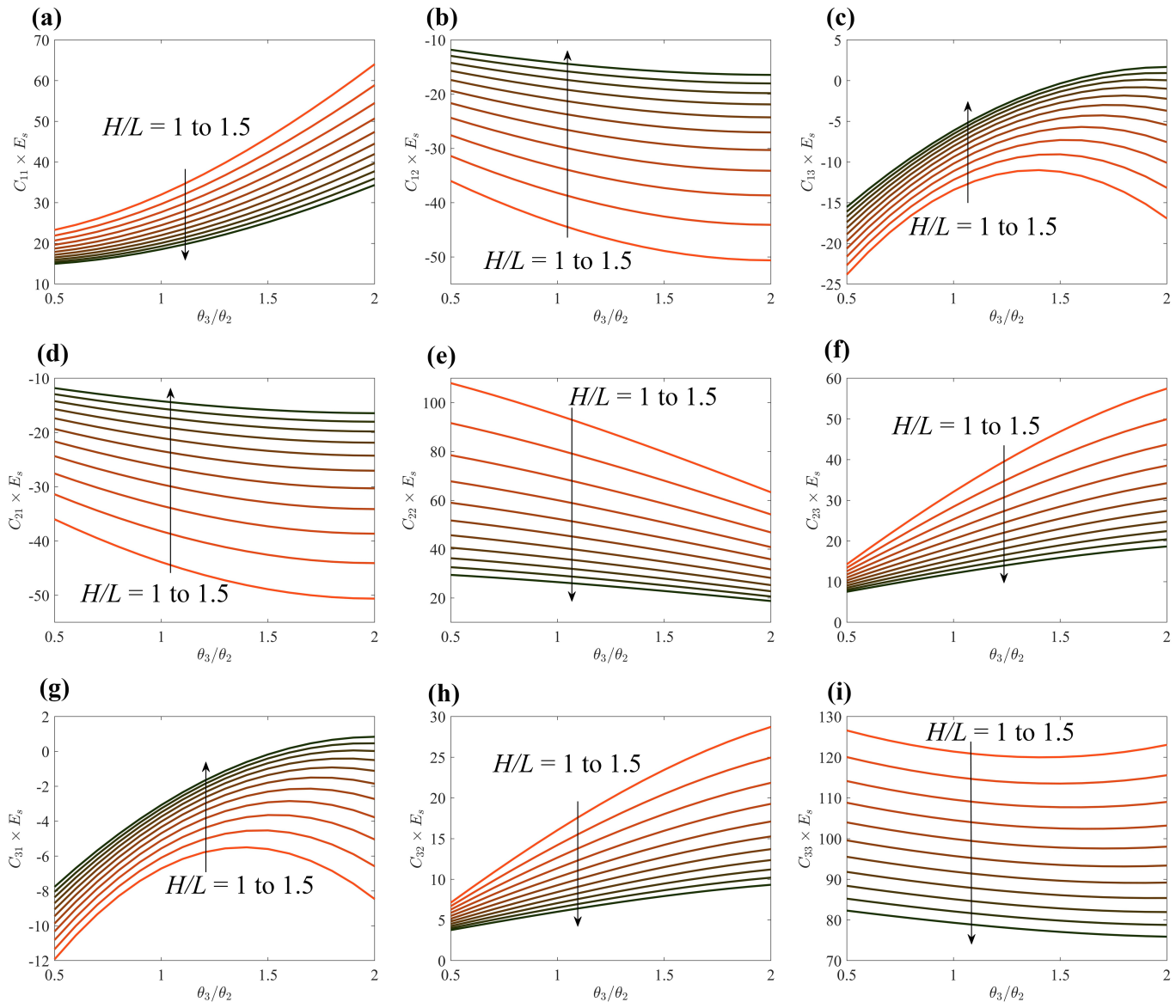

Figure 16: Effect of H/L ratio (ratio of the length of vertical and slant walls) on the complete in-plane constitutive (elastic modulus) matrix for non-auxetic multi-material variably-thickened cell wall asymmetric honeycombs under bending, axial and shear deformations. The non-dimensionalized values of elastic constitutive parameters for nonauxetic honeycombs ($E_1 = E_2 = qE_3 = E_s$, $L_1 = H = 1$ to 1.5mm, $L_2 = L_3 = L = 1$mm, $t_1 = t_2 = t_3 = 0.2L$, $\eta_1 = \eta_2 = \eta_3 = \eta = 0.5$, and $\zeta_1 = \zeta_2 = \zeta_3 = \zeta = 5$, $q = 2$) are plotted with angle ratio θ_3/θ_2 under the consideration of axial, bending and shear deformations of cell walls. The variation of constitutive constants is plotted for different H/L values with $\eta = 0.5$ and $\zeta = 5$. The normalization of the constitutive constants (C_{ij}) is carried out with respect to the intrinsic Young's modulus (E_s) of the vertical wall. Variations with respect to angle ratio θ_3/θ_2 considering different values of H/L are presented for **(a)** C_{11} **(b)** C_{12} **(c)** C_{13} **(d)** C_{21} **(e)** C_{22} **(f)** C_{23} **(g)** C_{31} **(h)** C_{32} **(i)** C_{33}. In these figures, the arrows depict an increasing trend of H/L from $H/L = 1$ to $H/L = 1.5$.

4. Conclusions and perspective

A computationally efficient, yet insightful analytical approach is developed here to determine the effective elastic constitutive properties of a novel class of bi-level architected lattice metamaterials. There are multiple notable facets (individually and their coupled influence) in the proposed lattice metamaterial that would improve the design space significantly: (1) the entire elastic constitutive matrix has been formulated considering the combined effect of bending, shear and axial deformation of the cell

walls (applicable for a wide range of lattices with thin to thick cell walls), (2) effect of multimaterial in the unit cells is introduced, (3) asymmetric designs in the unit cells are coupled with the multimaterial architecture, (4) beam-level variably-thickened architectures are proposed based on physical insights of stress resultants. In the proposed framework, first, the equivalent elastic moduli C_{12}, C_{22}, to C_{23} are determined for directions parallel to one cell wall of the variably-thickened multi-material honeycomb based on the beam level deformation mechanics. Further, the coordinate transformation is exploited to obtain all nine in-plane constitutive constants for asymmetric hexagonal honeycomb lattices.

A multi-stage validation approach, involving different beam-level deformation mechanics, multi-material parameters and asymmetry, is adopted to ascertain adequate confidence in the proposed analytical framework. Subsequently, a detailed numerical study is performed considering auxetic and non-auxetic configurations to explore the expanded design space of variably-thickened cell wall parameters η and ζ, multi-material parameter q, cell wall thickness and side lengths, and geometric parameters concerning asymmetry of the unit cell. The importance of considering axial and shear deformations along with bending is demonstrated for thicker cell walls in the lattices. The numerical results reveal that the variability-thickened cell wall parameters and the multimaterial parameter can alter all the in-plane constitutive constants of the non-auxetic and auxetic lattices without changing the basic unit cell geometry. Along with that, the coupled design space of asymmetry with auxetic and non-auxetic configurations would play a vital role in the design of next-generation highly optimized honeycomb structures for static and dynamic applications in various engineering fields.

Future research in this field will cover aspects beyond just weight reduction and stiffness-to-weight ratio, including the enhancement and control in a more expanded design space for specific strength and possibilities of localized failure in asymmetric geometries, stability, vibration and damping characteristics. Moreover, effective control over the auxetic behaviour and the prospect of achieving any type of functional properties gradation along the span can allow for desired effects such as improved impact resistance and energy absorption, enhanced structural stability under dynamic loads and shape conformability. In this context, the proposed concept of variably-thickened honeycomb design can further be investigated to enhance failure resistance through localized stiffening and strengthening along with improving the energy absorption capacity.

Besides the non-auxetic and auxetic configurations, the concept of current bi-level design can be exploited directly for analyzing a range of lattice forms such as rectangular and rhombic lattices with symmetric and asymmetric geometries, and further extended to other 2D and 3D lattices by considering appropriate unit cells. Following the proposed analytical framework, the design space can be significantly

expanded further by considering different cell wall thicknesses and parameters of variably-thickened cell walls (including consideration of continuous cell wall thickness variation) for the three cell walls. In addition, a range of other symmetric and asymmetric architectures can be introduced at the beam level as an extension of the current analytical framework. The disseminated generic concepts of this paper (including the computationally efficient analytical framework) would lead to exploitable physics-based insights for innovating topologically optimized multi-functional heterogeneous metamaterials with tailorable and direction-dependent elastic properties.

Supplementary materials

Supplementary Material 1 (SM1): In this Supplementary Material 1 (SM1), we present supplementary numerical results considering $t/L = 0.2$, encompassing (1) non-auxetic lattices with only beam-level bending deformation, and (2) auxetic lattices considering only beam-level bending deformation and the combined effect of beam-level bending, axial and shear deformations. Further, additional validation results are presented to reinforce the confidence in the current analytical framework.

Supplementary Material 2 (SM2): The results presented in the main paper and Supplementary Material 1 (SM1) are obtained for $t/L = 0.2$, unless otherwise mentioned. For a comprehensive understanding, we provide additional numerical results here for non-auxetic and auxetic honeycombs considering two other cell wall thicknesses, as $t/L = 0.1, 0.3$ (relatively thinner and thicker cell walls) with the variation of different bi-level geometric parameters such as θ, ζ, η, q, and H/L etc. (symmetric and asymmetric configurations).

Acknowledgments

MA acknowledges the financial support from the Ministry of Education, India through a doctoral scholarship. TM would like to acknowledge the Initiation grant received from the University of Southampton during the period of this research work.

Data availability

All data sets used to generate the results are available in the main paper. Further details could be obtained from the corresponding authors upon reasonable request.

References

[1] P. Sinha, T. Mukhopadhyay, Programmable multi-physical mechanics of mechanical metamaterials, Materials Science and Engineering: R: Reports 155 (2023) 100745.

[2] G. Hunt, T. Dodwell, Complexity in phase transforming pin-jointed auxetic lattices, Proceedings of the Royal Society A 475 (2224) (2019) 20180720.

[3] S. Khakalo, V. Balobanov, J. Niiranen, Modelling size-dependent bending, buckling and vibrations of 2d triangular lattices by strain gradient elasticity models: applications to sandwich beams and auxetics, International Journal of Engineering Science 127 (2018) 33–52.

[4] Y. Lai, Y. Wu, P. Sheng, Z.-Q. Zhang, Hybrid elastic solids, Nature materials 10 (8) (2011) 620–624.

[5] D. Kundu, S. Ghuku, S. Naskar, T. Mukhopadhyay, Extreme specific stiffness through interactive cellular networks in bi-level micro-topology architected metamaterials, Advanced Engineering Materials 25 (8) (2023) 2201407.

[6] S. Adhikari, T. Mukhopadhyay, A. Shaw, N. Lavery, Apparent negative values of young's moduli of lattice materials under dynamic conditions, International Journal of Engineering Science 150 (2020) 103231.

[7] T. Mukhopadhyay, S. Adhikari, A. Alu, Theoretical limits for negative elastic moduli in subacoustic lattice materials, Physical Review B 99 (9) (2019) 094108.

[8] T. Mukhopadhyay, D. Kundu, Mixed-mode multidirectional poisson's ratio modulation in auxetic 3d lattice metamaterials, Advanced Engineering Materials 24 (5) (2022) 2101183.

[9] D. Han, Y. Zhang, X. Y. Zhang, Y. M. Xie, X. Ren, Lightweight auxetic tubular metamaterials: Design and mechanical characteristics, Composite Structures 311 (2023) 116849.

[10] X. Ren, R. Das, P. Tran, T. D. Ngo, Y. M. Xie, Auxetic metamaterials and structures: a review, Smart materials and structures 27 (2) (2018) 023001.

[11] N. Feng, Y. Tie, S. Wang, J. Guo, A novel 3d bidirectional auxetic metamaterial with lantern-shape: elasticity aspects and potential for load-bearing structure, Composite Structures (2023) 117221.

[12] C. Luo, C. Z. Han, X. Y. Zhang, X. G. Zhang, X. Ren, Y. M. Xie, Design, manufacturing and applications of auxetic tubular structures: A review, Thin-Walled Structures 163 (2021) 107682.

[13] A. Sinha, T. Mukhopadhyay, Kirigami-inspired metamaterials for programming constitutive laws: Mixed-mode multidirectional auxeticity and contact-induced stiffness modulation, Iscience 25 (12).

[14] T. Mukhopadhyay, J. Ma, H. Feng, D. Hou, J. M. Gattas, Y. Chen, Z. You, Programmable stiffness and shape modulation in origami materials: Emergence of a distant actuation feature, Applied Materials Today 19 (2020) 100537.

[15] R. Tao, L. Ji, Y. Li, Z. Wan, W. Hu, W. Wu, B. Liao, L. Ma, D. Fang, 4d printed origami metamaterials with tunable compression twist behavior and stress-strain curves, Composites Part B: Engineering 201 (2020) 108344.

[16] Y. Zhang, L. Sun, X. Ren, X. Y. Zhang, Z. Tao, Y. M. Xie, Design and analysis of an auxetic metamaterial with tuneable stiffness, Composite Structures 281 (2022) 114997.

[17] B. R. Isanaka, T. Mukhopadhyay, R. K. Varma, V. Kushvaha, On exploiting machine learning for failure pattern driven strength enhancement of honeycomb lattices, Acta Materialia 239 (2022) 118226.

[18] A. Jha, G. Cimolai, I. Dayyani, Crashworthiness and dimensional stability analysis of zero poisson's ratio fish cells lattice structures, International Journal of Impact Engineering 184 (2024) 104809.

[19] J. Zhang, G. Lu, Z. You, Large deformation and energy absorption of additively manufactured

auxetic materials and structures: A review, Composites Part B: Engineering 201 (2020) 108340.

[20] X. Xiang, G. Lu, Z. You, Energy absorption of origami inspired structures and materials, Thin-Walled Structures 157 (2020) 107130.

[21] A. Bekele, M. A. Wadee, A. T. Phillips, Enhancing energy absorption through sequential instabilities in mechanical metamaterials, Royal Society Open Science 10 (8) (2023) 230762.

[22] P. Sinha, T. Mukhopadhyay, On-demand contactless programming of nonlinear elastic moduli in hard magnetic soft beam based broadband active lattice materials, Smart Materials and Structures 32 (5) (2023) 055021.

[23] A. Singh, S. Naskar, P. Kumari, T. Mukhopadhyay, Viscoelastic free vibration analysis of in-plane functionally graded orthotropic plates integrated with piezoelectric sensors: Time-dependent 3d analytical solutions, Mechanical Systems and Signal Processing 184 (2023) 109636.

[24] D. Kundu, S. Naskar, T. Mukhopadhyay, Active mechanical cloaking for unsupervised damage resilience in programmable elastic metamaterials, Philosophical Transactions of the Royal Society A.

[25] Z. Zhai, L. Wu, H. Jiang, Mechanical metamaterials based on origami and kirigami, Applied Physics Reviews 8 (4).

[26] H. Sharma, S. H. Upadhyay, Folding pattern design and deformation behavior of origami based conical structures, Advances in Space Research 67 (7) (2021) 2058–2076.

[27] R. M. Neville, F. Scarpa, A. Pirrera, Shape morphing kirigami mechanical metamaterials, Scientific reports 6 (1) (2016) 31067.

[28] Y. Yang, Z. You, Geometry of transformable metamaterials inspired by modular origami, Journal of Mechanisms and Robotics 10 (2) (2018) 021001.

[29] H. Sharma, S. Upadhyay, Geometric analyses and experimental characterization of toroidal miura-ori structures, Thin-Walled Structures 181 (2022) 110141.

[30] Q. Qin, I. Dayyani, Cylindrical helical cell metamaterial with large strain zero poisson's ratio for shape morphing analysis, Smart Materials and Structures 32 (10) (2023) 105039.

[31] S. A. Cummer, J. Christensen, A. Alù, Controlling sound with acoustic metamaterials, Nature Reviews Materials 1 (3) (2016) 1–13.

[32] A. Chaurha, P. Malaji, T. Mukhopadhyay, Dual functionality of vibration attenuation and energy harvesting: effect of gradation on non-linear multi-resonator metastructures, The European Physical Journal Special Topics 231 (8) (2022) 1403–1413.

[33] T. Tan, Z. Yan, H. Zou, K. Ma, F. Liu, L. Zhao, Z. Peng, W. Zhang, Renewable energy harvesting and absorbing via multi-scale metamaterial systems for internet of things, Applied Energy 254 (2019) 113717.

[34] J. Ji, Q. Luo, K. Ye, Vibration control based metamaterials and origami structures: A state-of-the-art review, Mechanical Systems and Signal Processing 161 (2021) 107945.

[35] M. Machado, B. Moura, S. Dey, T. Mukhopadhyay, Bandgap manipulation of single and multi-frequency smart metastructures with random impedance disorder, Smart Materials and Structures 31 (10) (2022) 105020.

[36] S. Dalela, P. Balaji, D. Jena, A review on application of mechanical metamaterials for vibration

control, Mechanics of advanced materials and structures 29 (22) (2022) 3237–3262.

[37] L. J. Gibson, Cellular solids, Mrs Bulletin 28 (4) (2003) 270–274.

[38] T. Mukhopadhyay, S. Adhikari, Stochastic mechanics of metamaterials, Composite Structures 162 (2017) 85–97.

[39] S. Ghuku, T. Mukhopadhyay, On enhancing mode-dependent failure strength under large deformation: The concept of anti-curvature in honeycomb lattices, Composite Structures 305 (2023) 116318.

[40] P. Prajwal, S. Ghuku, T. Mukhopadhyay, Large-deformation mechanics of anti-curvature lattice materials for mode-dependent enhancement of non-linear shear modulus, Mechanics of Materials 171 (2022) 104337.

[41] P. Sinha, M. Walker, T. Mukhopadhyay, Non-invariant elastic moduli of bi-level architected lattice materials through programmed domain discontinuity, Mechanics of Materials (2023) 104691.

[42] A. Singh, T. Mukhopadhyay, S. Adhikari, B. Bhattacharya, Extreme on-demand contactless modulation of elastic properties in magnetostrictive lattices, Smart Materials and Structures 31 (12) (2022) 125005.

[43] A. Singh, T. Mukhopadhyay, S. Adhikari, B. Bhattacharya, Active multi-physical modulation of poisson's ratios in composite piezoelectric lattices: on-demand sign reversal, Composite Structures 280 (2022) 114857.

[44] M. Wan, K. Yu, H. Sun, 4d printed programmable auxetic metamaterials with shape memory effects, Composite Structures 279 (2022) 114791.

[45] D.-H. Chen, K. Masuda, Equivalent elastic modulus of asymmetrical honeycomb, International Scholarly Research Notices 2011.

[46] D. Chen, L. Yang, Analysis of equivalent elastic modulus of asymmetrical honeycomb, Composite Structures 93 (2) (2011) 767–773.

[47] L. Zhang, B. Liu, Y. Gu, X. Xu, Modelling and characterization of mechanical properties of optimized honeycomb structure, International Journal of Mechanics and Materials in Design 16 (1) (2020) 155–166.

[48] M. A. Wadee, A. Phillips, A. Bekele, Effects of disruptive inclusions in sandwich core lattices to enhance energy absorbency and structural isolation performance, Frontiers in Materials 7 (2020) 134.

[49] K. Wei, Y. Peng, Z. Qu, Y. Pei, D. Fang, A cellular metastructure incorporating coupled negative thermal expansion and negative poisson's ratio, International Journal of Solids and Structures 150 (2018) 255–267.

[50] Z. Wang, J. Deng, K. Liu, Y. Tao, Hybrid hierarchical square honeycomb with widely tailorable effective in-plane elastic modulus, Thin-Walled Structures 171 (2022) 108816.

[51] B. Ling, K. Wei, Z. Wang, X. Yang, Z. Qu, D. Fang, Experimentally program large magnitude of poisson's ratio in additively manufactured mechanical metamaterials, International Journal of Mechanical Sciences 173 (2020) 105466.

[52] Y. Wu, Y. Lai, Z.-Q. Zhang, Elastic metamaterials with simultaneously negative effective shear modulus and mass density, Physical review letters 107 (10) (2011) 105506.

[53] Z. Liu, X. Zhang, Y. Mao, Y. Zhu, Z. Yang, C. T. Chan, P. Sheng, Locally resonant sonic materials, science 289 (5485) (2000) 1734–1736.

[54] G. W. Milton, M. Briane, J. R. Willis, On cloaking for elasticity and physical equations with a transformation invariant form, New Journal of Physics 8 (10) (2006) 248.

[55] J. Li, C. T. Chan, Double-negative acoustic metamaterial, Physical Review E 70 (5) (2004) 055602.

[56] H. Ding, Z. Zhen, H. Imtiaz, W. Guo, H. Zhu, B. Liu, Why are most 2d lattices hexagonal? the stability of 2d lattices predicted by a simple mechanics model, Extreme Mechanics Letters 32 (2019) 100507.

[57] T. Mukhopadhyay, A. Mahata, S. Adhikari, M. A. Zaeem, Effective elastic properties of two dimensional multiplanar hexagonal nanostructures, 2D Materials 4 (2) (2017) 025006.

[58] T. Mukhopadhyay, S. Adhikari, Free-vibration analysis of sandwich panels with randomly irregular honeycomb core, Journal of Engineering Mechanics 142 (11) (2016) 06016008.

[59] K. K. Gupta, L. Roy, S. Dey, Hybrid machine-learning-assisted stochastic nano-indentation behaviour of twisted bilayer graphene, Journal of Physics and Chemistry of Solids 167 (2022) 110711.

[60] T. Mukhopadhyay, S. Naskar, S. Adhikari, Anisotropy tailoring in geometrically isotropic multimaterial lattices, Extreme Mechanics Letters 40 (2020) 100934.

[61] D. Chen, X. Zheng, Multi-material additive manufacturing of metamaterials with giant, tailorable negative poisson's ratios, Scientific reports 8 (1) (2018) 1–8.

[62] P. Vogiatzis, S. Chen, X. Wang, T. Li, L. Wang, Topology optimization of multi-material negative poisson's ratio metamaterials using a reconciled level set method, Computer-Aided Design 83 (2017) 15–32.

[63] D. Kang, S. Park, Y. Son, S. Yeon, S. H. Kim, I. Kim, Multi-lattice inner structures for high-strength and light-weight in metal selective laser melting process, Materials & Design 175 (2019) 107786.

[64] M. Mirzaali, A. Caracciolo, H. Pahlavani, S. Janbaz, L. Vergani, A. Zadpoor, Multi-material 3d printed mechanical metamaterials: Rational design of elastic properties through spatial distribution of hard and soft phases, Applied Physics Letters 113 (24) (2018) 241903.

[65] H. Xu, D. Pasini, Structurally efficient three-dimensional metamaterials with controllable thermal expansion, Scientific reports 6 (1) (2016) 1–8.

[66] P. Tiwari, S. Naskar, T. Mukhopadhyay, Programmed out-of-plane curvature to enhance multimodal stiffness of bending-dominated composite lattices, AIAA Journal 61 (4) (2023) 1820–1838.

[67] D. Overaker, A. Cuitin o, N. Langrana, Elastoplastic micromechanical modeling of two-dimensional irregular convex and nonconvex (re-entrant) hexagonal foams 65 (3) (1998) 748–757.

[68] S. Mukherjee, S. Adhikari, A general analytical framework for the mechanics of heterogeneous hexagonal lattices, Thin-Walled Structures 167 (2021) 108188.